

# EVALUATING UNMANNED AERIAL VEHICLES FOR ATMOSPHERIC SCIENCE

BEN S. PICKERING  
21016940

DEPARTMENT OF METEOROLOGY, UNIVERSITY OF READING



*Submitted in partial fulfilment of the requirements for the degree of Master of Meteorology,  
Meteorology and Climate with a year in Oklahoma at the University of Reading, 10/03/2016.*

## ABSTRACT

This research aims to evaluate multi-rotor Unmanned Aerial Vehicles (UAVs) as a vertical profiling tool for atmospheric science. These are lightweight (less than 7 kg), remotely piloted aircraft with vertical-axis rotors. Atmospheric profiles of temperature, humidity and pressure are taken twice a day at thousands of locations across the globe and are heavily relied upon by weather forecasters and computer models. UAV technology has reached the price point and capabilities required to explore these new measurement techniques. Since technological advancements have outpaced airspace legislation, there is currently some uncertainty about the legality of UAV operations. This study placed temperature, humidity and pressure sensors onto a multi-rotor UAV and tested them in the lowest 120 m of the atmosphere at RUAO (Reading University Atmospheric Observatory). The BMP180 pressure sensor was shown to be highly correlated to RUAO data ( $R^2=1.00$ ). However, it was found that the SHT digital temperature and humidity sensors were poor. Despite moderate correlation with RUAO ( $R^2 = 0.62$  to  $0.94$ ), the slow response times ( $\tau_{0.63} = 292s$  to  $329s$  for temperature and  $\tau_{0.63} = 9s$  to  $485s$  for relative humidity) meant the sensors were unable to satisfy the hypotheses due to short UAV flight times. However, the thermistor response time ( $\tau_{0.63} = 6s$  to  $11s$ ) was fast enough to test the hypotheses, despite a large correction being required and the correlation to RUAO being moderate ( $R^2 = 0.51$  to  $0.71$ ). The thermistor was found to be a superior temperature sensor than the SHT for the aims of this research. Multiple profiles on 11/02/16 at RUAO showed realistic lapse rates. Statistical analysis of the UAV temperature data showed that the thermistor aboard the UAV was able to detect a temperature change between 10 m and 40 m above the surface. Rather than UAVs being an alternative to radiosondes, it was proposed that they could be used as a supplement to increase the density of lower atmospheric data in the future.

# 1. INTRODUCTION

## 1.1 ATMOSPHERIC PROFILING

Vertical profiles of the atmosphere are an important asset to forecasters and researchers alike, as they describe the properties and structure of the atmosphere in great detail. In addition, the retrieved data is fed into numerical models which predict the future state of the atmosphere.

There are multiple ways in which a vertical profile can be remotely obtained such as LiDAR or satellite, but as the tephigram in Figure 1 shows, satellite data is smoothed out compared to a radiosonde. This is due to the method used to retrieve the sounding, which can only measure the

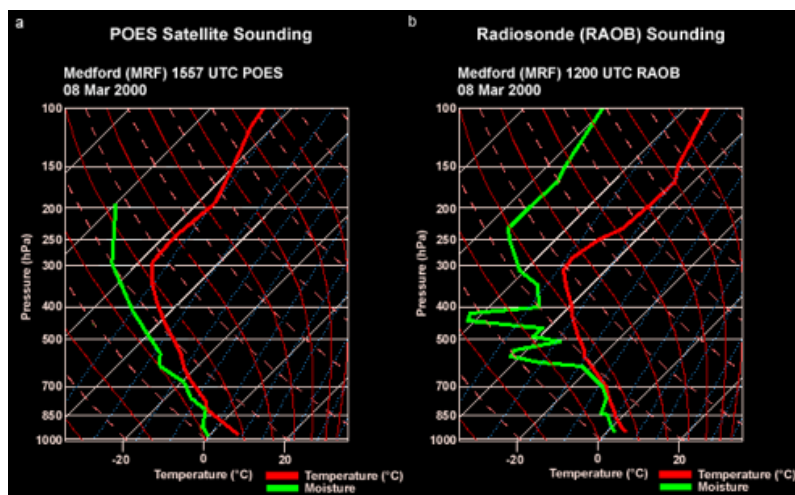


Figure 1: Atmospheric sounding obtained by (a) POES Satellite, and (b) Radiosonde Observations (RAOB). Courtesy of COMET® Program.

layer mean temperature. A significant disadvantage of remote sensing methods is that they cannot sense through clouds; however, an advantage is that (for the POES satellite) it can generate soundings for every 10 km of the atmosphere along its swath (Zapotocny et al., 2005). The radiosonde has in-situ single point data which is more accurate and resolves smaller features of the atmosphere such as the dry layers seen in Figure 1, but does not generate a true vertical profile as it drifts horizontally as it ascends, often more than 10 km. This horizontal motion adds complexity to the data which must be assimilated to a model grid for numerical weather prediction (NWP). Choi et. al (2015) showed that for a 4DVAR 6 km model, forecasts of meteorological variables such as horizontal wind components, temperature, and dewpoint temperature are improved by considering balloon drift information. Current operational models have grid spaces  $> 15$  km, hence the linear interpolation required to fit the radiosonde data to the grid introduces greater inaccuracies than that described in Choi et al., 2015.

Radiosonde packages such as that in Figure 2 measure temperature with a resistive bead thermistor, humidity with a hygistor (a glass plate covered with lithium chloride which has a moisture-dependant resistance) and pressure with an aneroid barometer (a sealed canister

which expands with pressure) (Hopkins, 1996). The thermistor and hygistor are separated from the unit to expose them to the airflow. There is an antenna to relay the data back to a

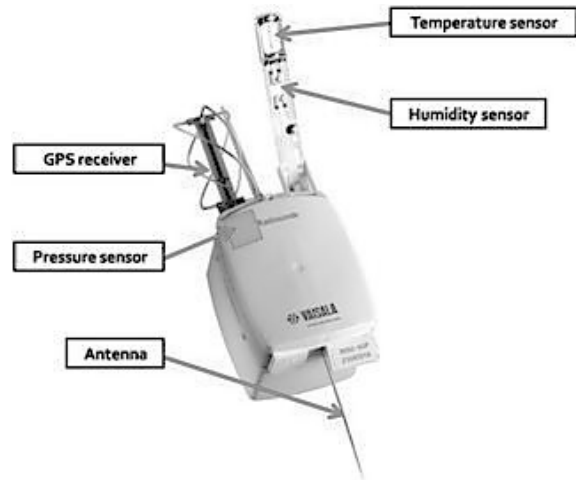


Figure 2: A labeled example of a typical radiosonde instrument package (Vaisala). Courtesy of Plymouth State University, Department of Atmospheric Science and Chemistry

ground station and modern radiosondes have a GPS unit which allows the wind speed and direction to be calculated throughout the ascent (technically this is a rawinsonde but the term radiosonde is used for both packages). The boxes are attached to helium or hydrogen balloons by at least 21 m of string which has been shown to reduce the thermal interference of the airflow around the balloon as it ascends (Schmidlin et al., 1986, Shimizu et al., 2010, Nash et al., 2011). This is currently the most

frequently used method for obtaining vertical profiles of the atmosphere, and occurs at least twice a day (00Z and 12Z) in the locations shown in Figure 3, which exceeds 1,500 sites, or approximately 1,000,000 launches every year. Radiosonde or rawinsonde ascents typically exceed the height of the tropopause, and depending on the elastic limit of the balloon can reach 35 km, at which point it may have drifted up to 200 miles horizontally from the launch site (NOAA, 2014). The cost of a radiosonde is around £150-£200 per launch, but the radiosonde ground station from Vaisala which is needed to calibrate the instrument package on the ground costs almost £50,000.

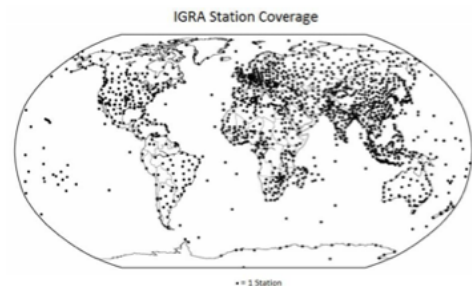


Figure 3: A map of the 1,500 IGRA (Integrated Global Radiosonde Archive) stations on Earth launching radiosondes (NOAA, 2014).

## 1.2 UNMANNED AERIAL VEHICLES

Technological advances and reduction of cost in the past two decades are responsible for the increase of consumer Unmanned Aerial Vehicles (UAVs) and Unmanned Aerial Systems (UAS), or “drones” as they are also known. These are small, Remotely Piloted Aircraft Systems (RPAS), often manufactured with computer assistance and autopilot functionality built-in. Figure 4 demonstrates a typical UAS setup of a UAV controlled by an operator with

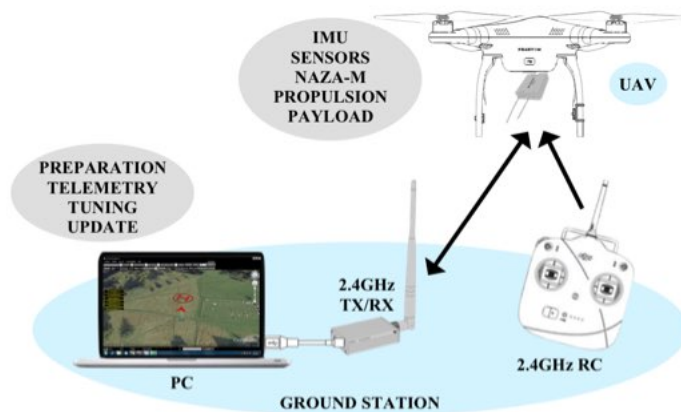


Figure 4: An example of the components used in an Unmanned Aerial System (UAS). The aircraft in the air is the Unmanned Aerial Vehicle (UAV) whilst the remote controller (RC), computer (PC) and additional transmitter/receiver are the Ground Station (GS). These components together make up the UAS.

a remote and a ground station receiving telemetry from the UAV and displaying the information on a PC. The ground station can be used to pre-program and upload waypoints for a flight to the UAV. Payloads for multi-rotor UAVs are typically lightweight cameras for consumer use, although scientific instrumentation for research purposes are increasingly being

tested. One of the benefits of using multi-rotor UAVs for atmospheric research compared to tethered balloons or fixed-wing UAVs is that multi-rotors can hover; this enables measurements to be taken over long periods of time and averaged for precision. This dampens perturbations and noise in the data caused by fluctuations in aircraft height or position, or turbulent eddies in the atmospheric boundary layer (ABL) which is where these craft are most suited to fly. Another advantage is the ability of the aircraft to manoeuvre freely in three dimensions, allowing profiles of any direction to be conducted in succession without interruption. Finally, UAS are reusable and therefore more sustainable than traditional radiosondes which are considered to be a single-use recording device. The number of radiosondes recovered is small and those reused are almost zero. Although latex balloons are made from the sap of rubber trees and are biodegradable in air, they are not biodegradable in water (Xian et al., 2008), where the majority of balloons will land (based on ocean-land surface ratio). Non-biodegradable materials are used to build the radiosonde instrument package, so irrespective of where they land these will not decompose. A published study from Australia found that 24 beach cleanups recovered 2460 weather balloons over 21 months, 70% of which landed in the Great Barrier Reef Marine Park (O'Shea et al., 2014). Latest publications attribute increasing levels of micro-plastics in oceans to degradation of the biosphere (Ivar do Sul et al., 2013, Baztan et al., 2014, Desforges et al., 2014).

Unclear legislation is a major limitation that has deterred scientists from conducting research with UAVs. Historically the model aircraft community have been largely policed by

themselves. However, the recent surge in popularity of consumer multi-rotor UAVs due to increased abilities and reduction of price presents legislators a problem. Rapid growth of the technology has outpaced laws designed to protect airspace (Oduntan, 2015). The dilemma is exacerbated by the lengthy legal process required for new legislation to be written, which often takes many years. Existing guidelines which exist for model aircraft have been applied to UAVs in the “*CAP 722 Unmanned Aircraft System Operations in UK Airspace – Guidance*” document produced by the Civil Aviation Authority (CAA) in the U.K. These define a small UAS as weighing less than 7 kg and do not require permission from the CAA to fly, but are restricted to 120 m above ground level flight, and no closer than 50 m to people or structures. Another important restriction is that the craft must remain in the line-of-sight of the operator at all times, which limits the usefulness of UAVs that could be used to relay information from a remote, inaccessible or dangerous location. For commercial work, the UAV operator must obtain a permit from the CAA. Despite no legitimate way to police the hobbyists, rules have been set out and legislators are in the process of determining how to enforce the proposed laws. The FAA (United States Federal Aviation Authority) in December brought into effect a requirement for all UAV owners to register their aircraft with an FAA database in the hopes that UAV owners can be traced in the event of an accident (FAA, 2016). Currently there is a fear of the “legal grey area”, whereas in the future scientific research with UAVs may be hindered due to license requirements and their associated cost.

Other limitations to the use of UAVs are the short flight times of around 20 minutes which also affects the range and height the aircraft can reach. This limits the use of current UAVs to measuring the ABL only, whereas fixed-wing UAVs can fly beyond this and radiosondes reach much higher altitudes. The perturbations from the spinning rotors and disturbed airflow of a multi-rotor UAV itself may impact the measurements taken on such a platform. This could be a major flaw of the system, if the ambient conditions are not reliably measured then the UAV is not suitable for conducting atmospheric research. One of the aims of this study is to quantify the impact of the multi-rotor UAV on the measurements which will determine the usefulness of this platform as a measuring device.

### **1.3 PRIOR RESEARCH**

Since the technology is relatively new, this is a novel area of research with only a handful of prior studies, which have mainly used fixed-wing UAVs instead of multi-rotors. A recent set of studies in the field of Meteorology have been conducted using the SUMO (Small Unmanned Meteorological Observer), a fixed-wing aircraft capable of recording profiles of the atmosphere through spiral ascensions over a minimum of 300m x 300m land area, up to 1500m above ground level (Reuder et al., 2009). UAS effectiveness for atmospheric research is discussed by Mayer et al. (2012), where parameterisation schemes in the AR-WRF (Advanced Weather Research and Forecasting) model are evaluated using the SUMO UAS. Thomas et al. (2012) demonstrated for the first time a fixed-wing UAV platform based turbulent water vapour flux measurement system. Further work by Wildmann et al. (2014) using multi-hole probes (MHPs) on the Meteorological Mini Aerial Vehicle (M<sup>2</sup>AV) showed that the fixed-wing UAV is capable of measuring atmospheric turbulence up to 20 Hz after optimisation. One of the few studies to utilise a multi-rotor UAV for Meteorology is Chang et al. (2016) which performed aerial sampling of volatile organic compounds with an octocopter. Electronically powered multi-rotor UAVs are suitable for this research since there are no aircraft exhaust fumes to interfere with the measurements and the aircraft is able to hover near a target area. The experiments comprised of hovering the aircraft with the attached sensors over a roadway tunnel shaft. The study showed the effectiveness of a multi-rotor UAV in collecting high quality atmospheric aerosol data.

The skill of multi-rotor UAVs in measuring atmospheric temperature and humidity data to generate vertical profiles akin to radiosondes is yet to be thoroughly tested in any published work. It is noted in Gonzalez et al. (2012) that there is a need for more cost-effective atmospheric vertical profiling instruments in an operational application due to governmental budget restrictions. Similar logic can also be applied to research, where funding-bodies are looking for efficiency and greater return on investment when allocating funding in an increasingly competitive domain with budget restrictions. These are issues that the recent advances in UAV technology have the potential to solve, which forms the motivation for this project.

## 1.4 PLAN

Multi-rotor aircraft will be used in this project to assess the effectiveness of this platform for atmospheric temperature and humidity data collection. The main hypothesis to test is:

*Multi-rotor unmanned aerial vehicles can be used as vertical profiling instruments for research and routine data collection.*

This is followed by four sub-hypotheses:

**1. *Aircraft exist that can carry payloads in vertical trajectories of the lower atmosphere.***

Consideration of the requirements for a suitable platform and an assessment of existing technology in regards to this will also occur. The UAV will be thoroughly tested to ensure safe operation. All aspects of the aircraft are assessed, including the battery time, performance in adverse weather and payload capacity. Maximum altitude is one of the key considerations for routine vertical profiling of the atmosphere, which is significant in terms of the hypothesis and therefore will be reviewed. Future technology will also be discussed, where theoretical advancements relate to and would benefit the hypotheses being tested. The airflow disturbance below the aircraft will depend on the power of the model chosen. This will be quantified to allow a Reynolds Number to be calculated and subsequently the flow regime (turbulent or laminar) will be discussed.

**2. *Sensors exist that are suitable for multi-rotor aircraft to carry as a payload.***

Firstly the appropriate sensors will be researched and chosen that suit the platform on which they will be flown, such as weight, resolution, accuracy, cost and advertised instrument error. Miniaturised sensor packages using Arduino circuit boards will be created, and open-source software will be utilised for programming the data logger. This system aims to be capable of recording temperature, humidity and pressure data. Extensive testing in an atmospheric chamber will ensure the sensors are performing acceptably before field testing begins.

**3. *Airflow of a multi-rotor UAV perturbs atmospheric measurements of temperature.***

The third sub-hypothesis is important for the quality and reliability of the data collected by UAVs. Figure 5 demonstrates the problem that air from above will be drawn downwards by



the rotors. At the same time, the aircraft will be generating heat; these two variables may balance to give an accurate representation of the atmosphere at the height of the aircraft. The purpose of the experiments undertaken in this research is to detect the bias of the aircraft measurements in comparison with a known truth at the same altitude in close proximity.

**4. Routine observations with instruments mounted on a multi-rotor UAS are feasible.**

All requirements for a UAV profiling instrument will be discussed in this report: social (legislation), economic (cost to build aircraft and sensors) and scientific (accuracy of data) concerns shall be addressed through the methodology laid out here.

Potential impacts of this research are an increase in vertical profiles recorded operationally on both spatial and temporal scales using UAVs. This would increase the data fed into forecast models for initialisation, particularly in the ABL. Additionally a more cost-effective method of recording vertical atmospheric profiles may be discovered, and further research involving UAVs as recording instruments could be conducted building upon the findings of this study.

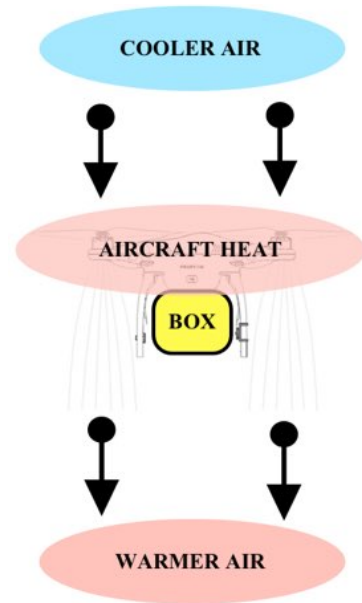


Figure 5: UAV heat fluxes for a typical atmospheric layer. The arrows indicate the direction of airflow caused by the aircraft operating.

## 2. METHODOLOGY

### 2.1 AIRCRAFT

The consumer leader in manufacturing multi-rotor UAVs is a company called DJI (Da-Jiang Innovations Science and Technology). They are responsible for a large portion of the growth in the personal drone industry with their *Phantom* line of quadcopter (4-rotor) UAVs intended for photographic purposes. For this research project, version 2 of the Phantom aircraft is used due to the low cost and advanced features which make it relatively easy to fly.

Table 1 shows that the DJI Phantom 2 has both useful features and negative hindrances in terms of the scientific objectives. The most important specification is the flight time which is advertised as 25 minutes, however the experiments will be conducted in January and February so the low temperatures may reduce this specification. The underperformance of Li-Po (Lithium Polymer) batteries in cold environments is well documented in the literature

*Table 1: DJI Phantom 2 technical specifications*

| SPECIFICATION                  | VALUE                |
|--------------------------------|----------------------|
| DIAGONAL WHEELBASE             | 350 mm               |
| AIRCRAFT HEIGHT                | 0.19 m               |
| AIRCRAFT WEIGHT <sup>1</sup>   | 1000 g               |
| MAX. WEIGHT                    | 1280 g               |
| MAX. BATTERY LIFE <sup>2</sup> | 25 Min ; 1500 s      |
| MAX. HORIZONTAL SPEED          | 15 m s <sup>-1</sup> |
| MAX. ASCENT SPEED              | 6 m s <sup>-1</sup>  |
| MAX. DESCENT SPEED             | 2 m s <sup>-1</sup>  |
| OPERATING TEMPERATURE          | -10 °C to +50 °C     |
| MAX. ALTITUDE <sup>3</sup>     | 6000 m               |

(Cho et al., 2012, Glaize and Genies, 2013, Zhu et al., 2015 and Jaguemont et al., 2016).

This will be thoroughly tested prior to the experimental flights. The maximum payload is defined in Table 1 by DJI as 280 g more than the aircraft weight. This is the value recommended by the manufacturer for the rest of the specification to be true; the payload can be higher but at the expense of battery time and flight speed. The target weight for the sensor package is therefore < 280 g. The aircraft is battery operated which means there are no exhaust gases to interfere with the measurements and heat generation is minimised. However, it is still necessary to consider the aircraft heat for the purposes of this research.

GPS hover lock is a feature of the Phantom 2 which reduces a source of human error and is useful to test the hypotheses, as the platform will remain stable without user input to an

<sup>1</sup> Aircraft weight with battery and all propellers included.

<sup>2</sup> Maximum battery life without additional components (i.e. when aircraft weighs 1000 g).

<sup>3</sup> Air density where aerodynamic lift becomes insufficient for hover.

accuracy of  $\pm 2.5$  m horizontally, and  $\pm 0.8$  m vertically using a barometer for altitude. This stability will ensure that any data anomaly is not due to the aircraft drifting.

The theoretical maximum altitude the aircraft could reach in a single flight is 2,250 m above the surface as it would take 375 seconds at the maximum speed of  $6 \text{ ms}^{-1}$  to ascend, and 1,125 seconds to descend at the maximum  $2 \text{ ms}^{-1}$  (limited to avoid vortex-ring state), for a total flight time of 1,500 seconds or 25 minutes as advertised. This specification will be reduced in colder temperatures where the battery will underperform or if the payload is greater than 280 g. This maximum profile height would allow measurements to be taken up to approximately 800 hPa, which allows an entire profile of the atmospheric boundary layer to be conducted during a single flight. However this would require special CAA permission, and therefore the research conducted here is limited to 120 m maximum altitude in accordance with CAA “*CAP 722 Unmanned Aircraft System Operations in UK Airspace – Guidance*” document discussed previously.

The downwash of the aircraft is the vertical component of the airflow that is generated by the rotors. This is important for the hypothesis of this experiment to ascertain the flow regime below the aircraft. This motion is not definitively quantified in this research but can be shown to be greater than the environmental vertical flow, which is measured on the order of  $1 \text{ m s}^{-1}$  in Hogan (2008). The original descent speed limit of the Phantom 2 was  $6 \text{ m s}^{-1}$ , but high reports of VRS from inexperienced users lead to a software update which introduced the  $2 \text{ m s}^{-1}$  limit. This tells us that the downwash from the UAV must be greater than  $2 \text{ m s}^{-1}$  whilst hovering and greater than  $8 \text{ m s}^{-1}$  when the aircraft is ascending at the maximum rate of  $6 \text{ m s}^{-1}$ . With this estimate, the flow regime below the aircraft can be calculated using the Reynolds Number, using the following equation:

$$\text{Re} = \frac{\rho V D}{\mu} = 1.27 \times 10^5 = 127000, \quad (1)$$

where  $\rho = 1.2 \text{ kg m}^{-3}$  is the density of air,  $V = 6 \text{ m s}^{-1}$  is the vertical velocity of the air past the aircraft (estimated whilst ascending),  $D = 0.35 \text{ m}$  is the characteristic distance (diameter of the aircraft) and  $\mu = 1.983 \times 10^{-5} \text{ Pa s}$  is the viscosity of air. Since  $\text{Re} \gg 4000$  the flow regime is turbulent, which means that there should not be a stagnation point below the aircraft, and we may assume the sensors are receiving a well-mixed flow. This ensures the measurements are as representative of the surrounding air as possible.

## **2.2 INSTRUMENTATION**

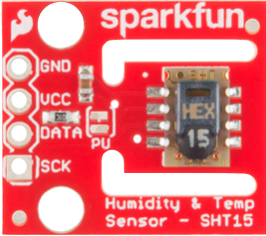

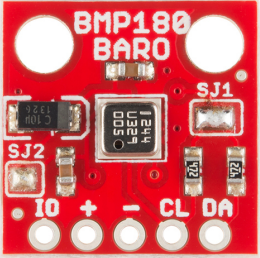
The instrumentation used in the experiments is of utmost importance to fulfil the outcomes of the research objectives. In particular, the error and resolution of the sensors need to be less than that of the range of variables expected in the experiments. Given the maximum flight altitude of 120 m above the surface, the pressure change ought to have a consistent range of  $\sim 15$  hPa. It would be optimal for the sensors to have a resolution 1 order of magnitude less than  $1\text{ }^{\circ}\text{C}$ , since this is the expected environmental lapse rate which may deviate from  $10\text{ K km}^{-1}$  if the meteorological conditions are not stable, or if the UAV disturbs the measurements. The range of relative humidity seen in the lowest 120 m of the atmosphere is difficult to estimate, since moisture at the surface and moisture transport flux in the atmospheric boundary layer are both widely fluctuating variables from day-to-day.

Another important consideration is the delay or lag time of the sensors. The battery life of the aircraft is relatively short, so the profiles up to 120 m will be relatively quick. The sensors must be able to acclimatise sufficiently as the UAV ascends, or produce a stable measurement before the aircraft is forced to descend. This is important to be able to determine whether the UAV is causing an offset in the measurements compared to fixed instruments at the same height, which is a sub-hypothesis of this research.

For comparison, both digital temperature and analogue temperature will be measured, as there are benefits from both. A thermistor is already used on operational radiosonde ascents because of their minimal lag time, however they are delicate; the vibrations of an operational re-usable UAS may damage the sensor over many flights, particularly during take-off and landing. Digital temperature sensors are more durable but this is at the expense of response time. Digital sensors are chip-mounted, and because of this, are typically slower to respond to change due to their thermal mass being larger than that of a bead thermistor. The sensors chosen for this research are detailed in Table 2.

The resolution of  $0.01\text{ K}$  in the SHT 15 sensor will allow precise measurements to be taken in the lowest 120 m of the atmosphere, where the expected change in temperature is expected to be around  $1\text{ K}$ . This resolution is 2 orders of magnitude lower than the expected environmental change and therefore is suitable for the research objectives to be satisfied. The thermistor has a lower resolution of  $0.14\text{ K}$  but the faster response time makes it a valuable

Table 2: Manufacturer specifications of the SparkFun SHT 15 digital temperature and humidity sensor, TDK B57540G1103+005 bead thermistor and BOSCH BMP 180 digital pressure sensor.

| SPECIFICATION                 | SHT 15   | THERMISTOR  | BMP 180  |
|-------------------------------|--|---|--|
| OPERATING VOLTAGES            | 2.4 V min<br>5.5 V max   | 18 mW max   | 1.8 V min<br>3.6 V max   |
| MEASUREMENT RANGE             | 0 - 100 % RH<br>-40 - 124 °C TEMP  | - 55 - 250 °C   | 300 - 1100 hPa<br>at -40 - 85 °C   |
| ABSOLUTE ACCURACY             | ± 2 % RH<br>± 0.3 K TEMP   | $\Delta R_{25}/R_{25} < 1 \%$   | ± 1.0 hPa  |
| RESOLUTION                    | ± 0.01 % RH<br>± 0.01 K TEMP   | 0.14 K  | 0.01 hPa   |
| RESPONSE TIME<br>$\tau$ (63%) | RH: 8 s<br>TEMP: 5 - 30 s  | 3 s   | 76.5 ms  |
| LONG TERM DRIFT               | < 0.5 % yr <sup>-1</sup><br>< 0.04 K yr <sup>-1</sup>                              | $\Delta R_{25}/R_{25} < 2 \%$<br>over lifetime                                      | ± 1.0 hPa yr <sup>-1</sup>   |
| APPROXIMATE COST              | ~ £30  | ~ £2  | ~ £7   |
| DESIGN                        |  |  |  |

component of the research. The thermistor data is recorded as a voltage  $V_0$  and converted to a usable temperature during the data analysis with the following equation:

$$T = b / \ln \left[ \frac{(V_{ref} \cdot R) - (V_0 \cdot R)}{V_0 \cdot a} \right], \quad (2)$$

where  $V_{ref} = 5$  volts,  $R = 5000 \Omega$ ,  $a = 0.040 \text{ K}^{-1}$  and  $b = 3625 \text{ K}$  (TDK, 2014). For humidity measurements, the 0.01 % resolution of the digital SHT chip is much higher than what is needed for vertical profiling, and the advertised response of 8 seconds is acceptable for the duration of the flight. Digital pressure sensors have been developed for many years and have reached a higher standard than the electronic temperature and humidity chips. Pressure measured by the BMP 180 has a response time comparable to a Vaisala radiosonde (VAISALA, 2016) and a resolution adequate for the purposes of converting into a height above the surface. The range of all the sensors chosen is acceptable with the possible exception of the SHT temperature measurement reaching -40 °C in extreme conditions. At

RUAO with a maximum height of 2.25 km, this should not pose an issue here, although it would be an issue for cold locations in the event of a global network of operational UAVs.

The data is linked to a timestamp and saved onto an SD card by the Arduino Uno, a small, lightweight programmable computer with 6 analogue inputs, 14 digital inputs and a CPU pre-installed. The Arduino is programmed with C and C++ code using the Arduino IDE. A program originally consisted of a real-time clock and logged the analogue ports (AN0-3) to an SD card (which uses ports AN4 and AN5); this code was courtesy of Prof. Giles Harrison, University of Reading. Further development of the code took many weeks and added the functionality of logging the SHT 15 and BMP 180 digital sensors to the SD card in the same string as the analogue ports with a timestamp. The code was streamlined by removing serial printing and unused libraries to make the measurement frequency faster, which appeared to be  $\sim 2.5$  Hz from a short test.

The approximate costs of the sensors are £40 together and the Arduino is £22 with the SD card reader module. The total cost of one sensor package is around £75 making it substantially cheaper than a radiosonde with the added benefit of being re-usable.

### 2.3 PROTOTYPE & CHAMBER TESTS

The prototype instrument shown in Figure 6 was tested in an atmospheric chamber to check sensor accuracy and response time. The temperature was adjusted from +30 °C to -12 °C over a time period of 20 minutes. This range is representative of those seen at the surface at RUAO in a typical year, and thus is the temperature range expected for an operational vertical profiling UAV within the ABL. The greater the maximum altitude of an operational aircraft, the more the sensors will need to be adapted to cold temperatures. The relative humidity of the atmospheric chamber was set constant at 50%, however the chamber does a poor job of maintaining RH. Figure 7 shows the results of the atmospheric chamber testing. The raw data from all sensors including the built-in chamber sensors are 1 minute averaged from 2.5 Hz to eliminate noise in the results.

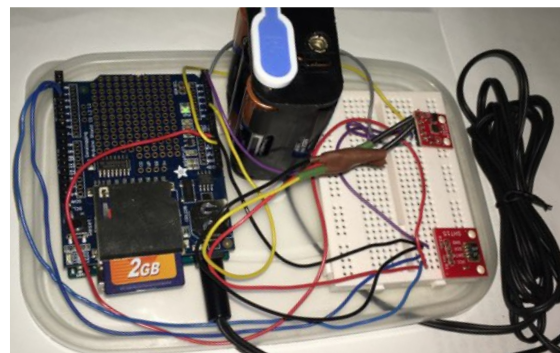


Figure 6: The prototype instrument package, with Arduino board and SD card left. The BMP 180 chip is top right, SHT 15 chip bottom right, and bead thermistor attached near the BMP 180.

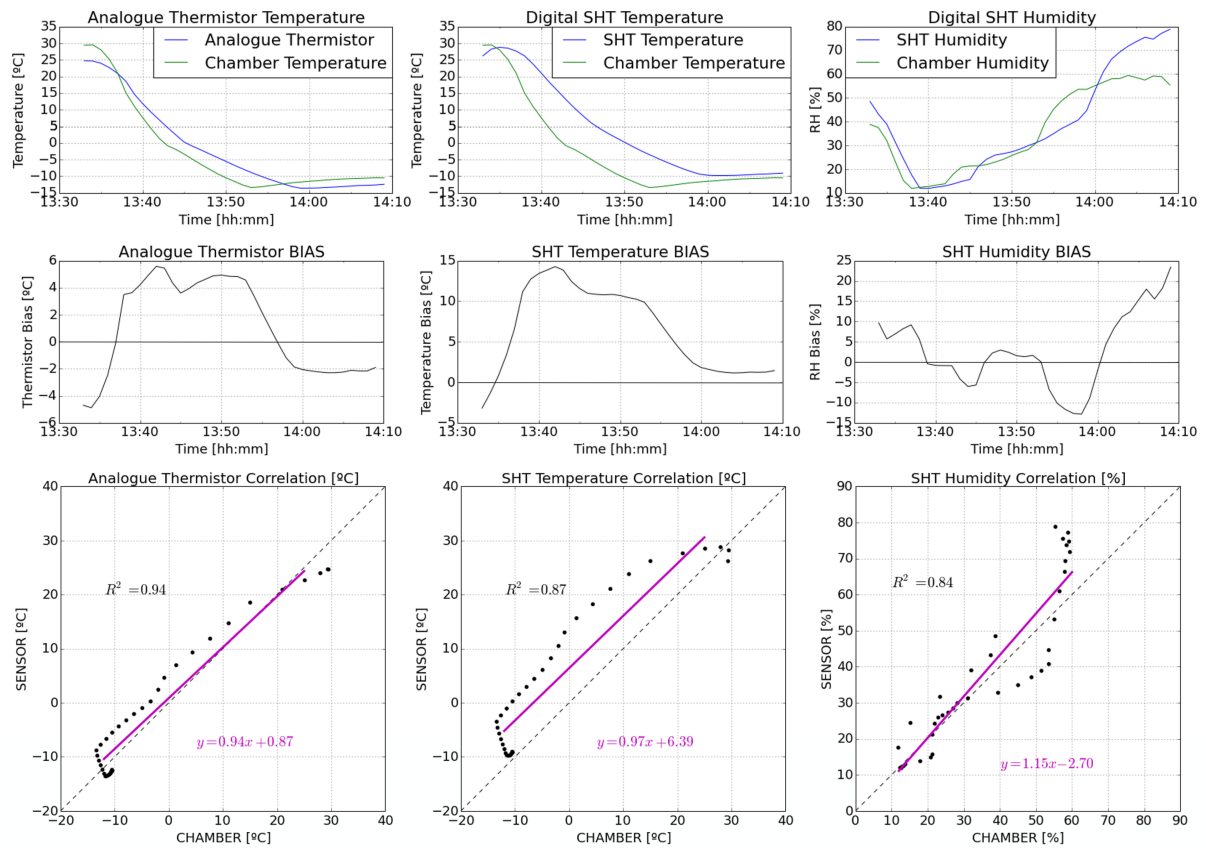


Figure 7: Atmospheric chamber testing on 30th Nov 2015. [Upper] Sensor and chamber data plotted over time. [Middle] Sensor bias calculated using sensor temperature minus chamber temperature. [Lower] Scatter plot of sensor and chamber data, with line of best fit in magenta and  $R^2$  correlation value displayed. [Left to right] Analogue thermistor temperature, digital SHT temperature, digital SHT relative humidity.

Figure 7 shows that for temperature, the bias is larger for the SHT chip compared to the thermistor, which is expected to be due to the slower response time due to the larger thermal mass of the SHT. Both temperature sensors experience a positive bias during the experiment, however the thermistor achieves a significant negative bias when the chamber temperature stabilises at -10 °C. The humidity sensor keeps a small bias in the early stages of the test, however as the temperature in the chamber becomes increasingly negative, the bias increases dramatically. This is a known problem where the change of phase of water below 0 °C affects the digital chip. This is a flaw in the system and means it will not be suitable for use as a vertical profiling instrument below 0 °C. The response time of the sensors will be considered in the following section.

Figure 8 shows the response time of the thermistor and digital temperature reading. The sensors are well acclimatised to the chamber reading before the door is opened and the sensors taken out. The light dashed horizontal line denotes the step-change from chamber to room temperature, with the bold dashed horizontal line denoting the  $\tau = 0.63$  value, which is when the sensor has measured 63% of the temperature change.

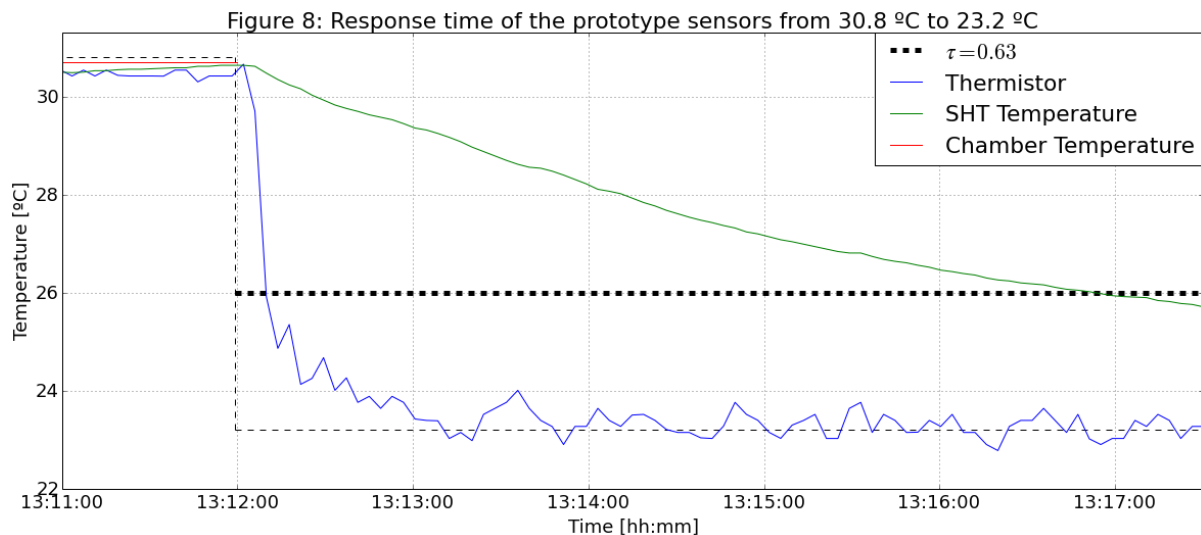


Figure 8: Atmospheric chamber testing on 30th Nov 2015. Response time of the thermistor and digital SHT to a step-change decrease in temperature. Step change represented by light black dashed line.

In Figure 8 the response time of the digital SHT 15 for temperature is poor. The measured response of 292 seconds is much larger than the 5-30 seconds advertised by the manufacturer. This may be exacerbated by the fact that the chip is in thermal contact with the breadboard it is plugged into. For this reason, the final design should attempt to separate the chip from the housing container as much as possible. If the response time during the experiments is 292 seconds, then the hypothesis cannot be thoroughly tested, as the sensor will not be able to reach a stable temperature within the time of a flight. The thermistor is responding to temperature as advertised given the proximity to the rest of the components in the prototype, which cools slower than the thermistor. A time response of 6 seconds makes the thermistor an ideal sensor to conduct the final experiment with. The hypothesis of detecting a bias in the data caused by the UAV requires a short sensor response time. The positive response time of the sensors are also tested for comparison, which is detailed in Table 3.



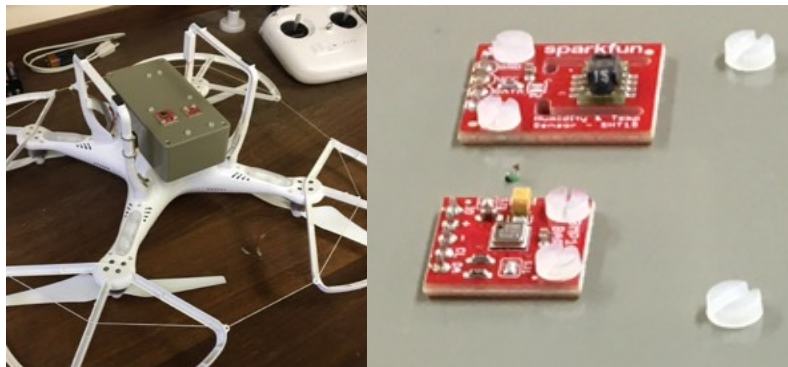
Table 3: Atmospheric chamber testing on 30th Nov 2015. Response time of all instruments excluding BMP 180 pressure. The first row is a decrease in temperature and a decrease in humidity, whilst the second row is an increase in temperature and decrease in humidity.

| <b>RESPONSE TIME<br/><math>\tau</math> (63%)</b> | <b>SHT TEMPERATURE</b> | <b>SHT HUMIDITY</b> | <b>THERMISTOR</b> |
|--|------------------------|---------------------|-------------------|
| <b>30.8 °C to 23.6 °C<br/>50 % to 42.6 %</b>     | <b>292 s</b>           | <b>9 s</b>          | <b>6 s</b>        |
| <b>15 °C to 25.7 °C<br/>50 % to 42.6 %</b>       | <b>329 s</b>           | <b>485 s</b>        | <b>11 s</b>       |

For the temperature increase from 15 °C to 25.7 °C seen in Table 3, the humidity increases initially as condensation forms on the chip, which then dissipates after 30 seconds. The decrease in temperature acts to dry the chip and therefore has the opposite effect than the condensation, and speeds up the response time. However, these two inappropriate tests do reveal a weakness of the sensor and demonstrate the worst and best case scenario for response. With this consideration, the best response time achieved is 9 seconds, which is close to the manufacturer quoted time of 8 seconds. This range of response time is a concern since the ability to test the hypotheses may be compromised. A more expensive RH sensor such as the dual sensor setup utilised on Vaisala radiosondes is known to have a faster response time, and is therefore more suitable for the experiments. The temperature sensors also perform slower for the increase in temperature compared to the decrease in temperature. This is significant because the vertical profile will be measuring a decrease in temperature as it ascends and an increase as it descends. Since they are unequal, the profile data cannot simply be averaged to overcome the lag. More complex combining techniques will be needed or sensors with faster response times should be used. In any case, the response time of all the sensors is slower than advertised, as they are not being tested in an ideal way to allow for the fastest response. However, these tests do show that the thermistor is capable of measurements quick enough to perform the experiments necessary to test the UAV temperature bias hypothesis. Therefore the results and discussion section of this report will focus on the thermistor sensor.

## 2.4 FINAL PACKAGE & FIELD TESTING

The final instrument packages is shown in Figure 9; the large grey box contains the Arduino board and SD card, all the sensors and the power supply. The battery is chosen to be a 9 volt PP3 based on a battery test where the voltage did not fall below 8.5 volts after 2 hours - the Arduino board demands a minimum of 5.03 volts to function. This is far greater than the advertised flight time of the aircraft which is 25 minutes. The total weight of the package is 222 g including the battery and SD card, which is comfortably within the 280 g aircraft payload limit recommended by the manufacturer. It was noted in the atmospheric chamber



*Figure 9: The final instrument package, with Arduino board, battery and SD card inside. On the right image, the BMP 180 chip is bottom, SHT 15 chip top and the bead thermistor is a green dot in between.*

tests that the thermal mass of the container housing the electronics and power supply was acting to slow the response of the measurements. To this end, a thin polystyrene sheet was secured below the SHT chip in an attempt to thermally isolate it and reduce

thermal conductivity with the box (not shown in Figure 9). Ideally, the electronic chips and thermistor would protrude further from the casing, however other considerations such as durability during landing and ease of access to the components inside the housing had to be taken into account. The design of the housing is structurally rigorous, which is aided by the 4 conveniently located screw holes on the aircraft itself which are intended to hold a camera gimbal. These screw holes are drilled in a trapezoid shape to maximise the rigidity of the attached object, which is beneficial in this experiment. There are three sensor packages in total; one each for the UAV, 10 m METFiDAS mast and the tethered balloon.

These three units were tested for agreement by placing them in a Stevenson screen at RUAO for 5 hours between 10:00 and 15:00 on 25th Jan 2016 and also between 17:00 and 23:59 on the 25th Feb 2016. The temperature ranges were 10-13 °C and 4-1 °C respectively. The results in Figure 10 show the process by which the boxes are tested and then calibrated to match the RUAO sensors, which are taken to be the ground truth in this study. Using two temperature ranges and averaging produced a more rigorous correction than a single dataset.

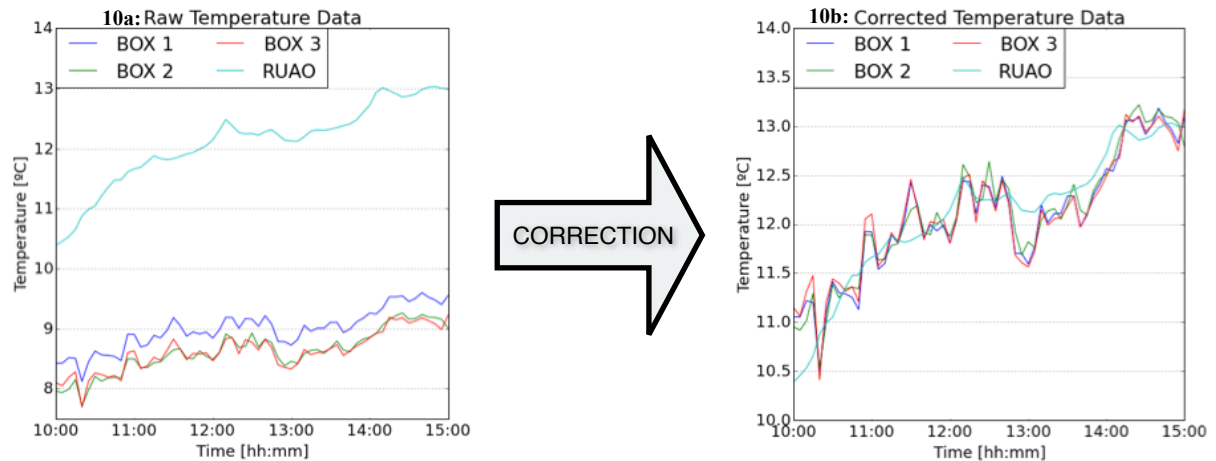


Figure 10: RUAO Stevenson screen testing on 25th Jan 2016. a) Raw thermistor data recorded by the 3 units b) the same data after Table 4 correction has been applied to fit the raw data to RUAO

| AVG CORRELATION                | BOX 1 - UAV                         | BOX 2 - MAST                        | BOX 3 - BALLOON                     |
|--------------------------------|-------------------------------------|-------------------------------------|-------------------------------------|
| <b>Digital Pressure</b>        | $y = 0.94x + 63.34$<br>$R^2 = 1.00$ | $y = 0.95x + 53.31$<br>$R^2 = 1.00$ | $y = 0.94x + 59.67$<br>$R^2 = 1.00$ |
| <b>Digital SHT Temperature</b> | $y = 1.26x - 5.76$<br>$R^2 = 0.78$  | $y = 1.35x - 6.67$<br>$R^2 = 0.80$  | $y = 1.23x - 6.37$<br>$R^2 = 0.62$  |
| <b>Analogue Thermistor</b>     | $y = 1.43x - 2.20$<br>$R^2 = 0.71$  | $y = 1.37x - 1.17$<br>$R^2 = 0.70$  | $y = 1.25x - 1.43$<br>$R^2 = 0.51$  |
| <b>Digital SHT Humidity</b>    | $y = 0.78x + 24.75$<br>$R^2 = 0.94$ | $y = 0.77x + 24.88$<br>$R^2 = 0.85$ | $y = 0.70x + 29.39$<br>$R^2 = 0.82$ |

Table 4: RUAO Stevenson screen testing on 25th Jan 2016 and 25th Feb 2016 averaged together. Least squares regression is used to produce the  $y=mx+b$  correction which is applied to the data to produce Figure 10b. Pearsons correlation statistic used to create  $R^2$  value in the table shows how correlated the measurements are to RUAO, where  $> 0.7$  is considered acceptable. See appendix for the non-averaged data.

Figure 10a shows the raw thermistor data from the the three instrument packages on 25/01/16; a Pearsons correlation was performed by each box against the RUAO data on both 25/01/16 and 25/02/16 and the data were averaged, the results of which are shown in Table 4. This transformation was then applied to each of the datasets to illustrate the effect of the correction on the data, which is to realign it to the RUAO data which is considered the ground truth. This is shown in Figure 10b. It should be noted that the raw thermistor data in Figure 10a shows that there is a large error up to  $-4\text{ }^\circ\text{C}$  between the thermistors and RUAO. By doing this correction process it is assumed that the range of values and rate of change of those values seen on 25/01/16 and 25/02/16 are representative of the values recorded during the main experiments with the UAV. This is not an ideal assumption; a more scientifically

sound method would be to average the corrections over a range of values from several datasets and over a longer period of time. If the sensors were to be accurate all year round at RUAO, extensive testing alongside RUAO instruments in an atmospheric chamber using multiple rates of change would be required. However, that is not possible within the limits of this research, so the discussed assumption was employed. Due to this, the error of  $\pm 4.0$  °C mentioned perviously must be retained as the error of any experimental temperature measurements. This is problematic since the expected environmental change during the experiments is less than 4 °C.

The  $R^2$  value for digital pressure was 1.00 meaning a perfect match with RUAO data. This clearly demonstrates the excellent technological progress that has been made in recent years with this class of sensor. The digital humidity and temperature sensors had good correlation, and the thermistor had moderate correlation. Despite the weaker correlation than the SHT temperature, the thermistor is still a superior sensor when lag time is taken into account. Taking everything into consideration, the digital SHT sensor will not be analysed in the results of this paper. This is because despite the good correlation with RUAO, the response times were simply too long to produce viable results by which to test the hypotheses. This means that pressure and thermistor temperature will be the only variables used in the results.

It is found that during the 5 hours in the Stevenson screen, the logging frequency of the three instrument packages varied between 2.44 Hz and 2.48 Hz, which is suitable for the purposes of this research. This was made possible by restructuring and trimming the Arduino logging code to be more efficient in the prototype. The logging frequency is not such that the amount of data for analysis is excessive; nor is the frequency too low to resolve minute changes in the observed variables. Instead, the logging frequency is such that fluctuations of the sensors may be quantified. These fluctuations may be caused through electrical interference and thermal conductivity, or more significantly, the influence of the airflow around the UAV disturbing the measurements. This experiment also confirmed that a 9 V PP3 battery is sufficient to power the Arduino for more than 6 hours, which is the duration of the proposed experiment where sensor packages are attached to the RUAO 10 m METFiDAS mast and 50 m tethered balloon.

In the following section the experimental procedure is explained as well as the rigorous safety precautions that were made before flying occurred.

## 2.5 EXPERIMENTAL PROCEDURE

In order to maintain a strict culture of safety regarding the experiments, a standard operating procedures (SOP) document was written as the first task of this research, as it is fundamental to the success of the project. An SOP document details the roles of the personnel on the ground and explains what they should do in the event of an emergency — a brief version exists in the appendix of this report. That document combined with a detailed risk assessment (see appendix also) was required to receive permission to fly on University of Reading Whiteknights campus. Checklists were carried



*Figure 11: Aerial map of the experiment site. RUAO enclosure in red, UAV take off point in white with a cross. Additional images of the experiment are in the appendix.*

out before any flight and the ground station allowed live telemetry to be analysed by the operator throughout the mission. The sensor package was firmly attached to the underside of the UAV as shown in Figure 9. Test flights on 18/01/16, 21/01/16 and 28/01/16 found that the manoeuvrability of the aircraft was not affected by the sensor package, and that the typical battery life in conditions less than 10 °C was around 13 minutes. These flights also resulted in numerous improvements to the operating procedures and checklists.

For the experiments on 11/02/16, the balloon instrument was tethered within the RUAO enclosure in Figure 11 with a string length of 50 m above ground level, and the METFiDAS mast instrument was in the centre of the enclosure at 10 m. The UAV take-off site was a wooden board with square dimensions of 1.5 m, which was placed southwest of RUAO indicated by the white box in Figure 11. The UAV did not deviate horizontally from this position; strictly moving vertically between the ground and 120 m which is the CAA limit for a UAV of this class (<7 kg). Multiple profiles were taken with the UAV as well as hovering for extended periods of time at the same height as the mast and the tethered balloon.

### 3. RESULTS

#### 3.1 METEOROLOGICAL CONDITIONS

Multiple experiments were conducted in an Intensive Observing Period (IOP) on 11/02/16 between 10:30 and 15:00. The meteorological conditions in Figure 12 show that the pressure trend measured by the control (RUAO) was decreasing. The temperature was between 6 °C and 7 °C during the IOP with maximum temperature of 7.7 °C at 12:30. Relative humidity decreased from 80 % at 11:00 to 65 % at 15:00. Cloud cover varied from 1/8th Ci to 5/8ths Cu which can be seen in Figure 12 as a drier, warmer period between 12:00 and 13:00.

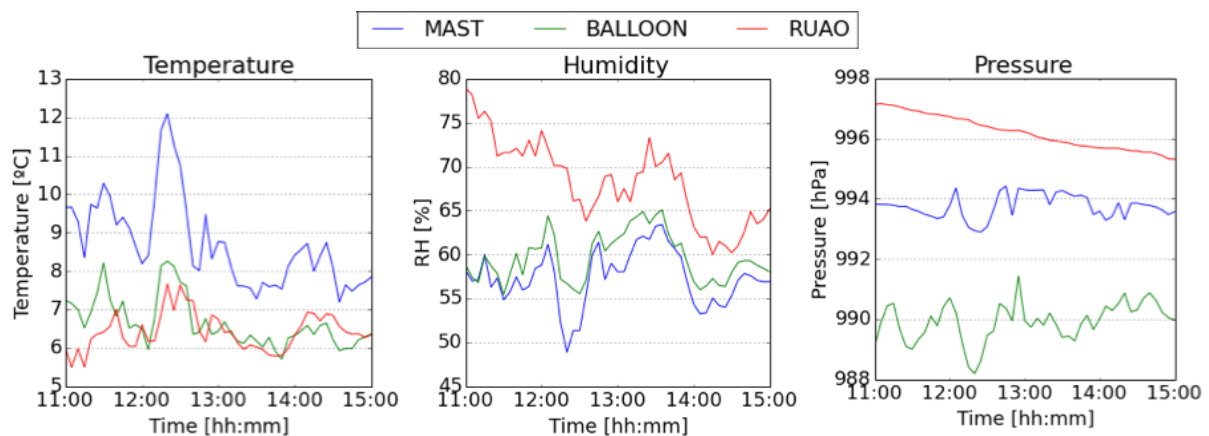


Figure 12: Meteorological conditions (5 min average) during the IOP on 11th Feb 2016.

The two custom-built sensor packages recorded the same shape as RUAO for temperature and humidity with offsets. Mast temperature was warmer than RUAO which may have been due to sunlight exposure. Balloon temperature was cooler than the mast which was expected since it was 40 m higher than the mast. Pressure measured by the mast and balloon were much more variable than that measured by RUAO. They were both exposed to the wind which might have affected the reading and the balloon began to drift later in the day as the wind speed increased. Balloon height fluctuated between 50 m and below 30 m which can explain some of the variance increase.

#### 3.2 VERTICAL PROFILES

4 vertical profiles of the ABL up to 120 m above the surface were taken throughout the IOP. Figure 13 shows the ascents and descents as solid and dashed lines respectively, where height has been calculated using the hydrostatic equation:

$$h = \frac{P_{UAV} - P_{RUAO}}{-\rho \cdot g}, \quad (3)$$

where  $P_{UAV}$  and  $P_{RUAO}$  are the pressure measured by the UAV and RUAO respectively,  $\rho = 1.2 \text{ kg m}^{-3}$  is the density of air and  $g = 9.81 \text{ m s}^{-2}$  is the acceleration due to gravity.

A lag in the measurements is noted by the disagreement between the ascent and descent portions of the flight. This separation can be somewhat attributed to the response time of the sensors, however it may also be due to the UAV and the airflow around it. As the aircraft ascends, the airflow through the rotors is greatly enhanced compared to a stable hover, since the rotors are spinning quicker creating a faster downwash. The opposite is true for the descent and the airflow through the craft slows. However, the data is not sufficient to explicitly quantify this effect.

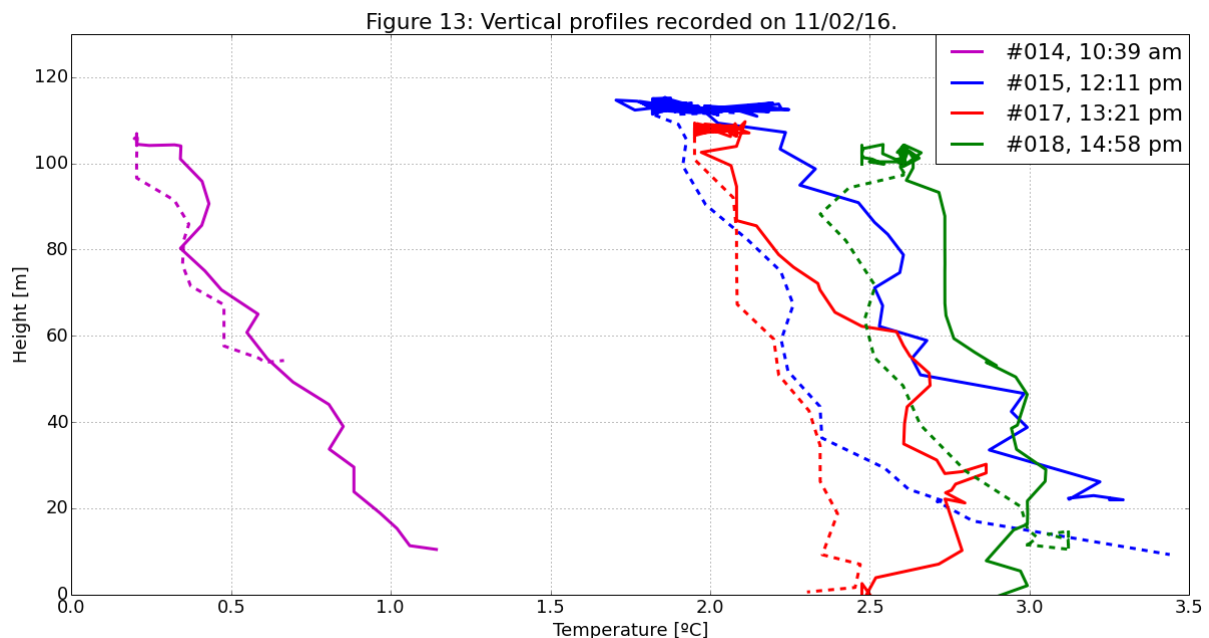


Figure 13: Vertical temperature profiles recorded on 11/02/16. The solid lines on the figure illustrate the ascent and the dashed lines represent the descent branch of the data.

The first profile of the day (Flight 014 at 10:39 am) was distinguished from the other profiles as a colder atmosphere existed at that time. The lapse rate was  $1 \text{ }^\circ\text{C}$  per  $100 \text{ m}$ , which is a realistic value. The profile at 13:21 pm had a similar gradient, but the 14:58 pm profile had a much shallower lapse rate. This suggests that the air above the surface had warmed whilst the surface had begun to cool. This could be explained by the increasing cloud cover noted throughout the day. The steepest lapse rate was at 12:11 pm but may be due to solar heating of the wooden landing platform which would raise the surface temperature measurement.

RUAO solar radiation data agrees with this diagnosis - there is an increase in incoming shortwave radiation at 12:11 pm which causes a dryer warm period as mentioned in section 3.1. For all of the profiles, the descent (denoted by the dashed line) is cooler than the ascent, which reinforces the suggestion that the separation is due to response time of the instrument. According to the aircraft telemetry, every profile was to 120 m, so Figure 13 demonstrates that the aircraft reading of height is unreliable, since it varies between 100 m and 115 m on these 4 profiles. The barometer inside the aircraft which relays the height data is susceptible to meteorological changes in atmospheric pressure, and hence the height (according to the aircraft) drifts over time even when the aircraft is stationary on the ground. The meteorological pressure change over the IOP is -2.0 hPa, or the equivalent of ~ 16 m decrease in height as represented by the quadcopter. This is by far the largest cause of uncertainty in the height measurements and therefore the error for this variable is  $\pm 8.0$  m.

Figure 13 does show that the UAV is able to realistically measure vertical temperature profiles in the atmosphere. However, these cannot be validated for accuracy since there is no true profile to compare against, only that the UAV is recording a change in temperature. Future research could use a tethered balloon or a slow radiosonde launch to generate a profile by which to compare the UAV data.

### **3.3 FLIGHT 016**

This flight was conducted between 12:56 and 13:11 during the IOP on 11/02/16 and consisted of an oscillatory height change between 10 m and 40 m, with 2 minutes spent at each height. The two heights are representative of a) the height of the METFiDAS mast and b) the estimated height of the tethered balloon, which, due to lack of helium and an increased wind speed had begun to drift and was therefore lower than the 50 m planned. The results in Figure 14 show the height of the UAV in black, which has an error of  $\pm 8.0$  m as discussed in section 3.2. This data shows that 3 periods occurred at 10 m, and 2 periods occurred at 40 m. The digital SHT sensors will not be discussed here as explained in section 2.4, justified by the poor response time.

During the aircraft warm up (UAV on the ground with rotors spinning) between 12:54:00 and 12:56:00, the pressure sensor shows an increase, which proves that the rotors are affecting the BMP 180 sensor. Simultaneously the thermistor records an 8 °C decrease in temperature from



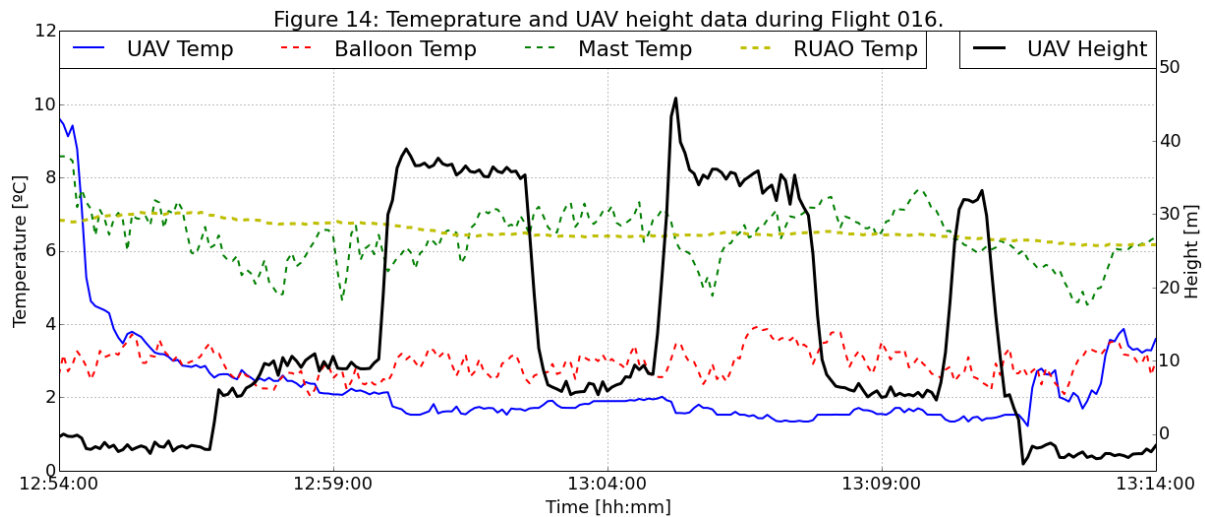


Figure 14: UAV height through flight 016 plotted simultaneously with the thermistor temperature measured by the UAV, METFiDAS mast and balloon instruments respectively. RUAO temperature is also plotted for reference. Uncertainty on the measurements are ignored for simplicity. RUAO is the control so uncertainty is zero. Height uncertainty as discussed in section 3.2 is  $\pm 8.0$  m. For the thermistor temperatures, error is quantified but noted to be too large to plot.

10 °C to 2 °C. The data recorded before the rotors are turned on is peaked which suggests that the wooden board being used as a launchpad is creating a positive bias in the temperature measurement, supporting the explanation given in section 3.2 for a steep lapse rate in Figure 13. The data is not reliable at this point in the flight, so the significance of the initial drop in temperature is unquantifiable. At take-off (12:56:00) the temperature reading from the thermistor is equivalent to the tethered balloon, which suggests that the UAV is drawing air from the balloon height to the ground. This seems unrealistic, as it is noted during the experiments that the height of the aircraft above the surface at which the grass below is disturbed is  $15 \text{ m} \pm 5 \text{ m}$  which if airflow symmetry is to be assumed, means that the fetch of the aircraft is not long enough to allow air cooler air from balloon height to be forced down. Evaporative cooling could account for some of the temperature drop, as the surface was moist from a morning ground frost. However, the platform from which the aircraft is launched is dry, so this effect ought to be minimal. This, combined with the  $\pm 4$  °C error in the thermistor measurements, makes the data unreliable and therefore difficult to interpret.

During the flight, the UAV thermistor temperature decreases sharply as the aircraft ascends, when the downwash of the aircraft was increased. This was not matched with a sharp increase in temperature when the aircraft descends. This suggests the UAV downwash is speeding up the response time of the thermistor. Longer flights with larger changes in height would

further test this explanation and could produce a more significant result. The temperature difference between the METFiDAS 10 m mast and the tethered balloon was 3-4 °C throughout the experiment. This seems large and lends further unreliability to the measurements. Despite that data appearing unreliable, the temperature variability was consistent with those expected due to turbulent eddies causing vertical wind speed fluctuations in the boundary layer (Hogan, 2008). This poses an issue with the experiment; the temperature fluctuations in the domain which is being measured are larger and more random than the expected effect of the UAV on the measurements. The UAV is essentially causing a small-scale turbulent eddy to form due to the downward motion of the air above and below the aircraft. This motion is discussed further in section 2.1 where it is proposed that the downwash of the aircraft is an order of magnitude greater than the environmental vertical flow.

In order to quantitatively say whether the UAV is able to record the change in temperature between 10 m and 40 m during Flight 016, a Student's *t*-test was conducted on the data plotted in Figure 14. The thermistor temperature data were separated into 2 sets, corresponding to a UAV height of 10 m and 40 m each. The first 2 minute period at 10 m height was removed due to the sensor not being fully acclimatised. The *t*-test assumes that the data are gaussian-distributed, which was verified. The mean and median of the two datasets are both < 0.03 °C apart and the skewnesses are both < 0.2. There is an issue that the data is slightly platykurtic; the kurtosis is -1.3 and -0.4 for 10 m and 40 m respectively. The sample size in each set is 44; Birnbaum and Zuckerman (1949) shows that a sample size > 30 is acceptable. It was determined that the *t*-test is statistically acceptable for the data. The results

Table 5: Results of *t*-test of the *t*-test are shown in Table 5.

|                |                             |   |
|----------------|-----------------------------|---|
| <b>T SCORE</b> | <b>5.86</b>                 | The null hypothesis in the test was that the datasets are insignificantly different. A small P-value means we can reject the null hypothesis and this tells us that there is a statistical significant difference between the datasets. Therefore it is proven that the UAV is able to detect a change in temperature between 10 m and 40 m. Further testing for longer flights with larger changes in height would enable a minimum detectable change to be revealed, however from this experiment it is clear that close to the surface, the UAV profiling instrument has a minimum |
| <b>P-VALUE</b> | <b>9.64x10<sup>-8</sup></b> |   |

detectable resolution less than 30 m, which is much finer than the resolution of typical tephigram. Figure 15 shows the two datasets in scatterplot and histogram form.

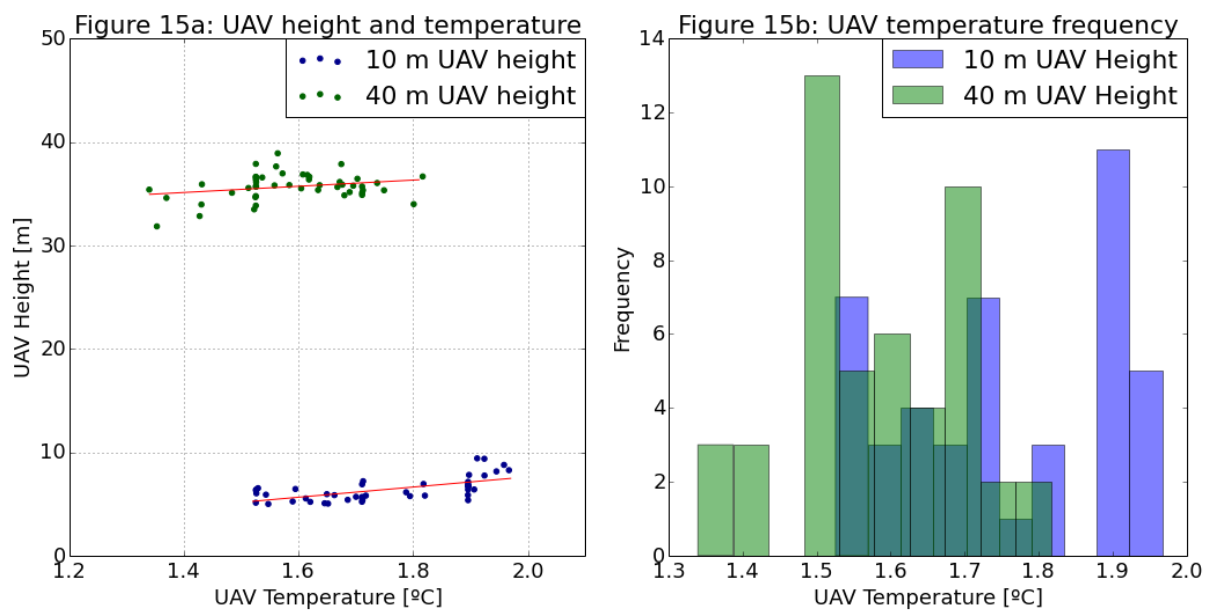


Figure 15: a) UAV temperatures at 10 m height in dark blue and recorded at 40 m in dark green.  
 b) A histogram of the temperature data in 15a with an identical colour scheme.

Figure 15a shows the temperature variability between the heights was homoscedastic, however, the height variability was heteroscedastic. The aircraft hovers less accurately at higher altitudes, as expected. Figure 15b shows that the temperature change with height was much smaller than Figure 14 described, although that change of 3-4 °C was questioned due to external influences. The mean temperatures recorded at 10 m and 40 m were 1.59 °C and 1.75 °C respectively. This corresponds to a lapse rate of 0.53 °C per 100m, which is far more realistic than Figure 14 suggested. This suggests the UAV is recording more accurately than previously thought, despite disagreeing with both the 10 m mast, 40 m balloon and RUAO.

## 4. DISCUSSION

### 4.1 AIRCRAFT ABILITIES

*Hypothesis: Aircraft exist that can carry payloads in vertical trajectories of the lower atmosphere.*

This research proves that recent technological advances have made UAVs capable enough to carry payloads in vertical trajectories of the lower atmosphere. The Phantom 2 is capable of experiments beyond those conducted in this research, which were limited by CAA safety restrictions. Despite this, an operational network of vertical profiling UAVs would require additional features that the Phantom 2 lacks. The inability to operate in precipitation is a huge disadvantage which is fundamental to an operational profiling instrument; a feature which is being added to many new consumer UAVs in 2016. The flight time can be improved although it is shown that profiles up to 2 km are possible with a Phantom 2 in warm weather. There are continual technological improvements being made in the UAV industry as a whole. The Phantom 2 was released in 2013, and since that time there have been improvements to the flight time within the company DJI, and further development from other companies. A research-centric UAV called the DJI Matrice 100 has an advertised battery-powered life of 40 minutes hovering (DJI, 2015) and a prototype hybrid gas-electric hexacopter “could carry a payload of 9 kg for 150 minutes” (MIT, 2015), making operational vertical profiles with larger payloads theoretically feasible to much higher altitudes in the future.

### 4.2 SENSORS

*Hypothesis: Sensors exist that are suitable for multi-rotor aircraft to carry as a payload.*

It is certainly true that sensors exist which are lightweight enough to be carried by current multi-rotor aircraft. The digital BMP180 pressure sensor far outperformed any other sensor. However, the poor response time of the SHT was a major flaw in the experiment, which has been partially attributed to it being in thermal contact with the box housing the electronics. Although the analogue bead thermistor had a slightly quicker response, it too suffered from the thermal insulating effect of the container and did not perform as advertised by the manufacturer. A future experiment should aim to distance the sensors away from the datalogger and isolate them from any thermal mass. The legs of the aircraft would be a more

suitable location, albeit at the expense of durability as the legs absorb most of the shock whilst the aircraft is landing. These changes would assist the sensors in performing at the advertised level, which was considered an acceptable level for the aims of this research. Although radiosonde sensor packages are expensive as discussed in section 1.1, they make very high quality measurements and are lightweight. For example, the Vaisala Radiosonde RS92-SGPL/D/A alone weighs between 160 and 290 grams depending on the type of battery used (VAISALA, 2013). This is proof that the technology exists to build a small, lightweight sensor package appropriate for UAVs, and thus could be developed in the future.

### **4.3 UAV PERTURBATIONS**

*Hypothesis: Airflow of a multi-rotor UAV perturbs atmospheric measurements of temperature.*

The results are inconclusive due to the large inaccuracies of the temperature sensors used in this research. Pressure is shown to be increased when the rotors are enabled, and a Reynolds Number calculation showed that the airflow is turbulent below the aircraft. This ensures the sensor receives a well-mixed atmospheric sample. Despite the inconclusiveness of the temperature results in Flight 016, section 3.2 showed that the aircraft is able to generate realistic vertical profiles (albeit with large variability), and section 3.3 proved that the aircraft was able to detect a temperature change between 10 m and 40 m height above the surface.

### **4.4 ROUTINE OBSERVATIONS**

*Hypothesis: Routine observations with instruments mounted on a multi-rotor UAS are feasible.*

Dense networks of observations are required to support higher resolution numerical models in the future. To this end, UAVs are well suited to a scale-up in network density (if the legislation can be successfully navigated), whereas radiosondes have stricter physical constraints surrounding their launch site. It is shown in this report that UAVs can be cheaper than radiosondes due to reusability. The two obstacles limiting a future network of vertical profiling UAVs are legislation and development of higher-quality sensors.

## 5. CONCLUSION

This research aimed to evaluate multi-rotor UAVs as a vertical profiling tool for atmospheric science. Currently available technology is shown to have reached the level of reliability, price point and flight time for this aim to be tested and future technology is postulated to improve the competence of UAVs for vertical profiling.

A digital BMP180 sensor was shown to be highly correlated to RUAO data ( $R^2=1.00$ ). However, it is found that the SHT digital temperature and humidity sensors are poor for a vertical profiling UAV. Albeit moderate correlation with RUAO ( $R^2 = 0.62 - 0.94$ ), the slow response times ( $\tau_{0.63} = 292s - 329s$  for temperature and  $\tau_{0.63} = 9s - 485s$  for RH) restrict the sensors for the intended purpose due to short flight times (approx. 13 minutes) in cold weather. The thermistor response time ( $\tau_{0.63} = 6s - 11s$ ) is fast enough for the aims of this research. However, a large correction is required and the correlation to RUAO is only moderate ( $R^2 = 0.51 - 0.71$ ) and therefore the measurement uncertainty is  $\pm 4.0$  °C, greater than the environmental change in the experiments. The delicate nature of the thermistor makes it prone to shock damage during rough landings, however, it is also 10x cheaper than the digital chips and therefore easily replaceable.

Multiple profiles on 11/02/16 at RUAO showed realistic lapse rates. Statistical analysis of the UAV temperature data showed that the thermistor aboard the UAV was able to detect a change in temperature between 10 m and 40 m above the surface. Conducting this experiment in the lowest 50 m of the surface boundary layer made it impossible to decipher between turbulent fluctuations and aircraft influence to determine the cause of the measured temperature bias. Near the surface there are many complex unpredictable processes occurring which externally influence the experiment and add variables to consider. A more rigorous test would be conducted in the free atmosphere where external influences are minimised. This would enable the bias caused by the aircraft to be identified.

Rather than UAVs being proposed as a cheaper replacement to balloons, they should be seen as a cheaper way to increase the density of vertical profile ascent data. This is because they cannot yet replace balloon radiosondes at high altitudes, but they can achieve a greater spatial and temporal resolution within the atmospheric boundary layer, which will be necessary for

higher resolution modelling in the future. Balloons are not as scaleable as UAVs because they currently require more manpower and have stricter criteria for a launch location.

Future work should focus on humidity measurements using dual-sensor setups similar to radiosondes. Legislation is an essential piece of any UAV operation and should be the first consideration in any research using them. Law is constantly changing and this poses a risk to future researchers if changes make a UAS unfeasible after development, which means it is vital to keep up-to-date on this matter. The technology advances in this industry are shown to be outpacing legislation, and it is therefore equally important to pay attention to new developments that will benefit this area of research.

## 6. REFERENCES

- Baztan, Juan, Ana Carrasco, Omer Chouinard, Muriel Cleaud, Jesús E. Gabaldon, Thierry Huck, Lionel Jaffrès, et al. 2014. Protected areas in the atlantic facing the hazards of micro-plastic pollution: First diagnosis of three islands in the canary current. *Marine Pollution Bulletin*, **80 (1-2)**: 302-11.
- Birnbaum, Z. W., and H. S. Zuckerman, 1949. A graphical determination of sample size for Wilks' tolerance limits. *The Annals of Mathematical Statistics*, **20 (2)**: 313-6.
- CAA (Civil Aviation Authority), 2004. CAP 722 Airspace Unmanned Aerial Vehicle Document, <http://publicapps.caa.co.uk/modalapplication.aspx?appid=11&mode=detail&id=415>. Accessed 3rd February 2016.
- Chang, Chih-Chung, Jia-Lin Wang, Chih-Yuan Chang, Mao-Chang Liang, and Ming-Ren Lin. 2016. Development of a multicopter-carried whole air sampling apparatus and its applications in environmental studies. *Chemosphere* **144** : 484-92.
- Cho, Hyung-Man, Woo-Sung Choi, Joo-Young Go, Sang-Eun Bae, and Heon-Cheol Shin. 2012. A study on time-dependent low temperature power performance of a lithium-ion battery. *Journal of Power Sources*, **198** : 273.
- Choi, Yonghan, Jong-Chul Ha, and Gyu-Ho Lim. 2015. Investigation of the effects of considering balloon drift information on radiosonde data assimilation using the four-dimensional variational method. *Weather and Forecasting*, **30 (3)**: 809-26.
- Desforges, Jean-Pierre W., Moira Galbraith, Neil Dangerfield, and Peter S. Ross. 2014. Widespread distribution of micro-plastics in subsurface seawater in the NE pacific ocean. *Marine Pollution Bulletin*, **79 (1-2)**: 94-9.
- DJI (Da-Jiang Innovations Science and Technology Co., Ltd., 大疆创新科技有限公司), 2013. Phantom 2 Diagram, *Phantom 2 User Manual*, 4-5, [http://download.dji-innovations.com/downloads/phantom\\_2/en/PHANTOM2\\_User\\_Manual\\_v1.00\\_en.pdf](http://download.dji-innovations.com/downloads/phantom_2/en/PHANTOM2_User_Manual_v1.00_en.pdf). Accessed October 2015.
- DJI (Da-Jiang Innovations Science and Technology Co., Ltd., 大疆创新科技有限公司), 2015. Matrice 100 Specifications, <http://www.dji.com/product/matrice100/info#specs>. Accessed 21st February 2016.
- FAA (Federal Aviation Authority), 2016, Unmanned Aircraft Systems (UAS) Registration, <https://www.faa.gov/uas/registration/>. Accessed 23rd February 2016.
- Glaize, Christian, and Sylvie Genies. 2013. *Lithium batteries and other electrochemical storage systems*. 1st ed. Hoboken: Wiley-ISTE.
- Gonzalez, L., Kos, L., Lavas, S., Douglas, M., (2012), A new possible plan for a more cost-effective adaptive radiosonde observing strategy for the United States, *Journal of Atmospheric and Oceanic Technology*. **2012**, 25 p.p.
- Hogan, R., (2008), 4. The Turbulence Closure Problem, *Lecture notes distributed in MT36E Boundary Layer Meteorology at the University of Reading*, Figure 1, p8, [http://www.met.rdg.ac.uk/~swrhgnrj/teaching/MT36E/MT36E\\_BL\\_lecture\\_notes.pdf](http://www.met.rdg.ac.uk/~swrhgnrj/teaching/MT36E/MT36E_BL_lecture_notes.pdf). Accessed 20th February 2016.
- Hopkins, Edward J., (1996). Radiosondes - An Upper Air Probe, *University of Wisconsin, Department of Atmospheric and Oceanic Sciences*, <http://www.aos.wisc.edu/~hopkins/wx-inst/wxi-raob.htm>. Accessed 6th February 2016.



- Ivar do Sul, Juliana A, and Monica F. Costa. 2013. The present and future of microplastic pollution in the marine environment. *Environmental Pollution (Barking, Essex : 1987)*, **185** : 352.
- Jaguemont, J., L. Boulon, and Y. Dubé., (2016). A comprehensive review of lithium-ion batteries used in hybrid and electric vehicles at cold temperatures. *Applied Energy*, **164**, 99-114.
- Mayer, S., Sandvik, A., Jonassen., M., O., Reuder, J., (2012), Atmospheric profiling with the UAS SUMO: a new perspective for the evaluation of fine-scale atmospheric models. *Meteorol. Atmos Phys*, **116**: 15-26.
- MIT (Massachusetts Institute of Technology), March 2015. Hybrid Power Could Help Drone Delivery Take Off, *Technology Review*, <https://www.technologyreview.com/s/535951/hybrid-power-could-help-drone-delivery-take-off/>. Accessed 21st February 2016.
- Nash, J., T. Oakley, H. Vömel, L. Wei, WMO Intercomparison of High Quality Radiosonde Systems, Yangjiang, China, 12 July - 3 August 2010, *Instruments and Observing Methods*, **107**, [http://www.wmo.int/pages/prog/www/IMOP/reports/2003-2007/RSO-IC-2005\\_Final\\_Report.pdf](http://www.wmo.int/pages/prog/www/IMOP/reports/2003-2007/RSO-IC-2005_Final_Report.pdf). Accessed on 6th February 2016.
- NOAA (National Oceanic and Atmospheric Administration), July 2014. Radiosondes, *JetStream - Online School for Weather*, <http://www.srh.noaa.gov/jetstream/upperair/radiosondes.htm>. Accessed 6th February 2016.
- NOAA, September 2014, Figure 3: Integrated Global Radiosonde Archive (IGRA) Station Locations, *National Centres for Environmental Information*, <https://www.ncdc.noaa.gov/data-access/weather-balloon/integrated-global-radiosonde-archive>. Accessed 8th February 2016.
- Oduntan, Gbenga., 2015, The age of drones has arrived quicker than the laws that govern them. *The Conversation*, <https://www.kent.ac.uk/law/research/news/?view=905>. Accessed 23rd February 2016.
- O'Shea, Owen R., Mark Hamann, Walter Smith, and Heidi Taylor. 2014. Predictable pollution: An assessment of weather balloons and associated impacts on the marine environment--an example for the great barrier reef, Australia. *Marine Pollution Bulletin*, **79 (1-2)**: 61-8.
- Plymouth State University, June 2010, Figure 2: Labeled Radiosonde Diagram, *Department of Atmospheric Science and Chemistry*, <https://www.plymouth.edu/department/asc/files/2010/06/sonde1.jpg>. Accessed 6th February 2016.
- Reuder, J., Brisset, P., Jonassen, M., Müller, M., Mayer, S., (2009), The Small Unmanned Meteorological Observer SUMO: A new tool for atmospheric boundary layer research. *Meteorologische Zeitschrift*, **Vol. 18**, 141-147.
- Schmidlin, F. J., J. K. Luers, and P. D. Huffman, 1986. Preliminary estimates of radiosonde thermistor errors. *NASA Technical Paper 2637*, 15 pp.
- Shimizu, K. and Hasebe, F., 2010, Fast-response high-resolution temperature sonde aimed at contamination-free profile observations. *Atmos. Meas. Tech.*, **3**, 1673-1681, doi:10.5194/amt-3-1673-2010.
- TDK, August 2014, Glass-encapsulated sensors, standard type, *NTC thermistors for temperature measurement*, Page 5, <http://docs-europe.electrocomponents.com/webdocs/13c1/0900766b813c1e91.pdf>, Accessed 7th February 2016.
- Thomas, R. M., K. Lehmann, H. Nguyen, D. L. Jackson, D. Wolfe, and V. Ramanathan. 2012. Measurement of turbulent water vapor fluxes using a lightweight unmanned aerial vehicle system. *Atmospheric Measurement Techniques*, **5 (1)**: 243-57.

- UCAR (University Corporation for Atmospheric Research), 2015. Introduction to Remote Sensing 2.4.1.1: Sounder versus Radiosonde. *MetEd COMET Program*, [https://www.meted.ucar.edu/tropical/textbook\\_2nd\\_edition/navmenu.php?tab=3&page=4.1.2](https://www.meted.ucar.edu/tropical/textbook_2nd_edition/navmenu.php?tab=3&page=4.1.2). Accessed 6th February 2016.
- VAISALA, 2013. Radiosonde RS92-SGP Datasheet <http://www.vaisala.com/Vaisala%20Documents/Brochures%20and%20Datasheets/RS92SGP-Datasheet-B210358EN-F-LOW.pdf>. Accessed 21st February 2016.
- Wildmann, N., S. Ravi, and J. Bange. 2014. Towards higher accuracy and better frequency response with standard multi-hole probes in turbulence measurement with remotely piloted aircraft (RPA). *Atmospheric Measurement Techniques*, **7 (4)**: 1027-41.
- Xian, Choo Mei, Chou Lee Yiung, Manju Latha Krishna Moorthy, and Siti Zata. 2008. Why don't we plant a tree instead? *New Straits Times*, **2008**.
- Zapotocny, Tom H., W. Paul Menzel, James A. Jung, and James P Nelson III. 2005. A four-season impact study of rawinsonde, GOES, and POES data in the eta data assimilation system. part I: The total contribution. *Weather and Forecasting*, **20 (2)**: 161-77.
- Zhu, Gaolong, Kechun Wen, Weiqiang Lv, Xingzhi Zhou, Yachun Liang, Fei Yang, Zhilin Chen, et al. 2015. Materials insights into low-temperature performances of lithium-ion batteries. *Journal of Power Sources*, **300** : 29-40.

## 7. APPENDICES

### 7.1 FLIGHT LOG

*For flights during the IOP only.*

**Pilot Name: Ben Pickering**

| Date | Launch time (local) | Landing time (local) | Flight duration (mins) | Location | Battery flown | Battery voltage pre flight (V) | Battery voltage post flight (V) | Weather | Flight path                                 | Max height (m)   | Observations |                           |
|------|---------------------|----------------------|------------------------|----------|---------------|--------------------------------|---------------------------------|---------|---|--|--------------|---------------------------|
| #014 | 11/02/16            | 10:39                | 10:50                  | 11       | SW of RUAO    | 184                            | 12.4                            | 10.3    | 4/8ths Ci, Cs<br>6°C 75%<br>200° 2m/s       | profile to 120m, 1 min, 50 m, 3 mins,                    | 120m         | 7m at ground              |
| #015 | 11/02/16            | 12:11                | 12:24                  | 13       | SW of RUAO    | 078                            | 12.4                            | 10.8    | 4/8ths Ci, Cu<br>in distance                | profile to 120m,<br>hover 8 mins                         | 120m         | 4m at ground              |
| #016 | 11/02/16            | 12:56                | 13:11                  | 15       | SW of RUAO    | 184                            | 12.2                            | 10.3    | 1/8th Ci, 3/8<br>ths Cu, more<br>Cu forming | 10m 2 mins, 40 m<br>2 mins, 10m 2 mins<br>40m 2 mins 10m | 40m          | 4m at ground              |
| #017 | 11/02/16            | 13:21                | 13:32                  | 11       | SW of RUAO    | 078                            | 12.2                            | 10.4    | 1/8ths Ci, 4/8<br>ths Cu,<br>broken Cu      | profile to 120m,<br>hover 5 mins                         | 120m         | 1.2m at ground            |
| #018 | 11/02/16            | 14:58                | 15:12                  | 14       | SW of RUAO    | 184                            | 12.4                            | 10.4    | 5/8ths Cu                                   | profile to 120m,<br>hover 5 mins                         | 120m         | 5m at start<br>10m at end |
|      |                     |                      |                        |          |               |                                |                                 |         |   |  |              |                           |
|      |                     |                      |                        |          |               |                                |                                 |         |   |  |              |                           |
|      |                     |                      |                        |          |               |                                |                                 |         |   |  |              |                           |

## 7.2 CORRECTION DATA

Separate correction data for 25/01/16 and 25/02/16.

| <b>25/01/16</b>                | <b>BOX 1 - UAV</b>                  | <b>BOX 2 - MAST</b>                 | <b>BOX 3 - BALLOON</b>              |
|--------------------------------|-------------------------------------|-------------------------------------|-------------------------------------|
| <b>Digital Pressure</b>        | $y = 0.97x + 26.38$<br>$R^2 = 1.00$ | $y = 0.98x + 18.02$<br>$R^2 = 1.00$ | $y = 0.98x + 16.32$<br>$R^2 = 1.00$ |
| <b>Digital SHT Temperature</b> | $y = 1.51x - 8.19$<br>$R^2 = 0.95$  | $y = 1.64x - 10.27$<br>$R^2 = 0.92$ | $y = 1.69x - 10.63$<br>$R^2 = 0.91$ |
| <b>Analogue Thermistor</b>     | $y = 1.82x - 4.28$<br>$R^2 = 0.82$  | $y = 1.74x - 2.89$<br>$R^2 = 0.87$  | $y = 1.81x - 3.51$<br>$R^2 = 0.77$  |
| <b>Digital SHT Humidity</b>    | $y = 0.73x + 26.29$<br>$R^2 = 0.94$ | $y = 0.69x + 29.33$<br>$R^2 = 0.93$ | $y = 0.70x + 28.01$<br>$R^2 = 0.93$ |

Table 6a: Correction data for 25th January 2016.

| <b>25/02/16</b>                | <b>BOX 1 - UAV</b>                   | <b>BOX 2 - MAST</b>                 | <b>BOX 3 - BALLOON</b>               |
|--------------------------------|--------------------------------------|-------------------------------------|--------------------------------------|
| <b>Digital Pressure</b>        | $y = 0.90x + 100.29$<br>$R^2 = 0.99$ | $y = 0.91x + 88.59$<br>$R^2 = 1.00$ | $y = 0.90x + 103.01$<br>$R^2 = 0.99$ |
| <b>Digital SHT Temperature</b> | $y = 1.01x - 3.32$<br>$R^2 = 0.61$   | $y = 1.05x - 3.07$<br>$R^2 = 0.68$  | $y = 0.76x - 2.11$<br>$R^2 = 0.32$   |
| <b>Analogue Thermistor</b>     | $y = 1.04x - 0.11$<br>$R^2 = 0.60$   | $y = 0.99x + 0.56$<br>$R^2 = 0.52$  | $y = 0.68x + 0.65$<br>$R^2 = 0.24$   |
| <b>Digital SHT Humidity</b>    | $y = 0.82x + 23.20$<br>$R^2 = 0.69$  | $y = 0.84x + 20.43$<br>$R^2 = 0.77$ | $y = 0.70x + 30.77$<br>$R^2 = 0.70$  |

Table 6b: Correction data for 25th February 2016.

## 7.3 STANDARD OPERATING PROCEDURES

*This is an excerpt from the full document:*

### **Flight team**

A minimum of two crew members (Pilot and Commander/Ground Control Assistant) are required to operate the UAV in flight. An additional third person may be employed as a safety spotter. The pilot must have had previous flying experience (at least 5 hours flight time) and must familiarise themselves with the aircraft being flown (through study of the instruction manuals and ideally time on a flight simulator), as well as the current CAA regulations involving UAV flights.

### **Role of the pilot**

- The pilot is responsible for the control of the UAV during flight
- The pilot has the authority to give commands he or she deems necessary in the interest of the safety of persons, property or the UAV
- The pilot is responsible for the execution of the flight within the realms of CAA regulations and for flying within the airspace permissions of the flying location.
- The pilot is responsible for completing the post flight log book (example shown in *Appendix*)

### **Specific guidelines when operating in manual mode**

- Before flying the pilot should ensure that the controller is in GPS mode
- The pilot should be in control of the UAV at all times and should fly the UAV in a safe manner
- If the UAV is not under control in GPS mode then manual ATTI mode should be used

### **Specific guidelines when operating in autopilot mode (using waypoint software)**

- The pilot should be prepared at all times to take over manual control of the UAV
- After take-off the pilot should maintain visual contact with the UAV for as long as possible, and simultaneously monitor the UAV through ground station
- The pilot should maintain regular checks of the airspace for other aircraft, changing weather conditions and other hazards

### **Role of the Ground Control Assistant (GCA)/ Commander/ Spotter**

- The GCA is responsible for assisting the pilot in the duties associated with collision avoidance and informing the pilot of any notable sightings or sounds
- The GCA is responsible for the operation of the ground station
- The GCA is responsible for downloading science data from sensors after a flight

### **Specific guidelines when operating in manual mode**

- The GCA shall act as the role of spotter when in manual mode, maintaining visual contact with the UAV
- The GCA will also monitor airspace for infringement by other aircraft, changing weather conditions or other hazards

### **Specific guidelines when operating in autopilot mode (using waypoint software)**

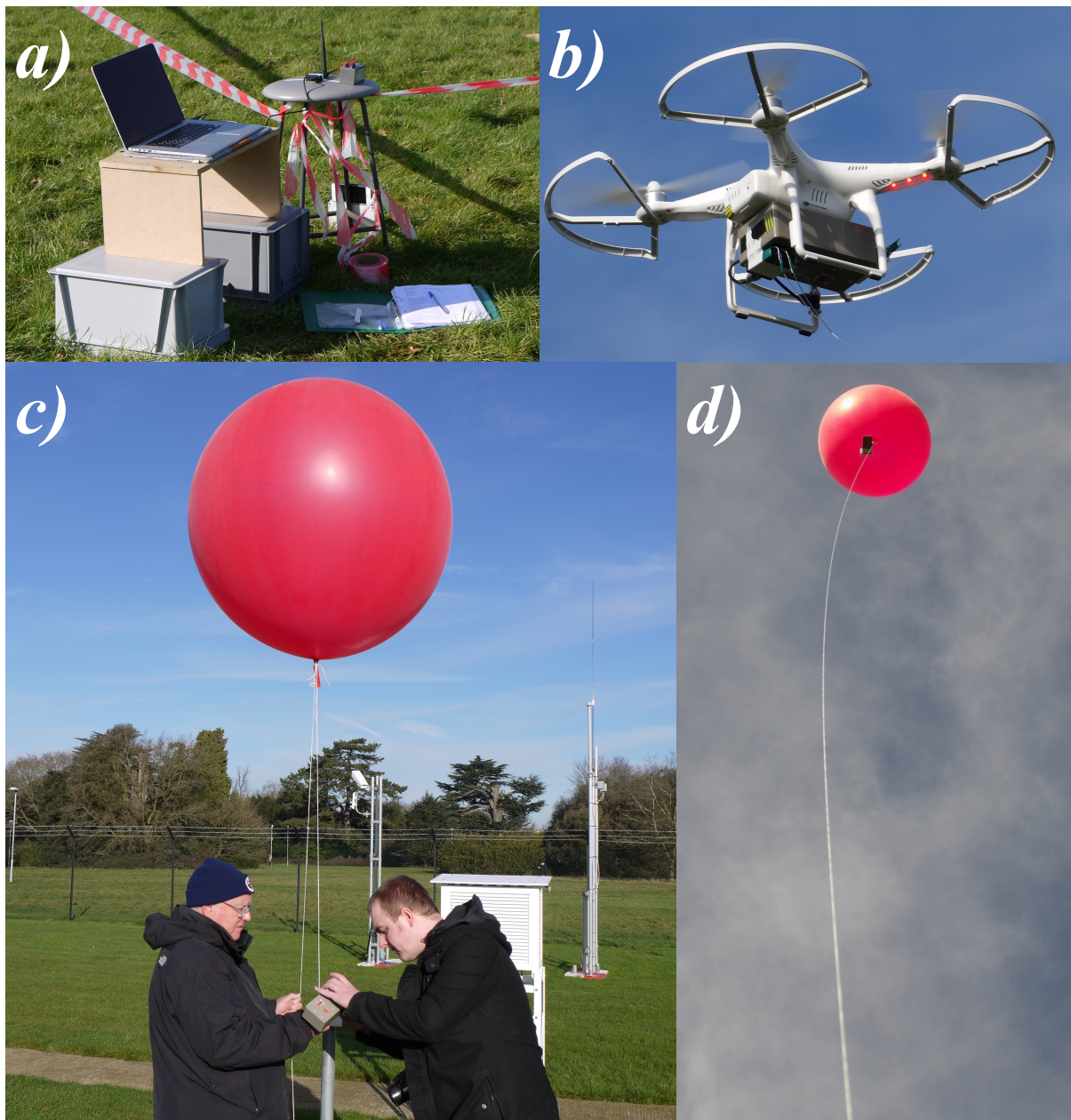
- The GCA should ensure flight plan is uploaded to UAV correctly and that the home position is correct
- The GCA should ensure correct execution of flight plan during flight by continuous monitoring of UAV performance (including position, airspeed, battery voltage) through ground station.
- The GCA will keep the pilot informed of approaching waypoints, descents, deviations from routes and general information that might be of interest to the pilot

## 7.4 RISK ASSESSMENT

### Small Unmanned Aerial Vehicle (SUAV) work

| Name of person undertaking assessment  | Name of Fieldwork Supervisor         | Date conducted  | Location and description of SUAV measurements being undertaken   |                          |                                     |                                     |   |
|--|--------------------------------------|---|--|--------------------------|-------------------------------------|-------------------------------------|---|
|  |                                      |   |  |                          |                                     |                                     |   |
| Date of UAV flights  | Flying location                      | Persons who may be affected by the activity (i.e. the risk)   |  |                          |                                     |                                     |   |
|  |                                      |   |  |                          |                                     |                                     |   |
| <b>Section 1 : Identify Hazards - Consider the activity or work area and identify if any of the hazards listed below are significant (tick the boxes that apply)</b> |                                      |   |  |                          |                                     |                                     |   |
| Hazard No.   | Hazard description                   | Associated risk   | Key control measures   | Risk level (tick one)    |                                     |                                     | Further actions needed to reduce risks<br>(provide timescale and initials of persons responsible) |
|  |                                      |   |  | High                     | Med                                 | Low                                 |   |
| 1.   | <b>Live electrical components</b>    | Electric shock risk   | Plastic housing around UAV discourages contact with live components. UAV battery is 11V therefore no significant shock risk.   | <input type="checkbox"/> | <input type="checkbox"/>            | <input checked="" type="checkbox"/> |   |
| 2.   | <b>Unexpected propeller start-up</b> | Injury to fingers/hands   | Propeller guards around all propellers minimise potential for contact with spinning blades. Training through operational flight checklists. Always start up in manual mode. First aid kit carried for every flight. Wear gloves when handling propellers.  | <input type="checkbox"/> | <input checked="" type="checkbox"/> | <input type="checkbox"/>            |   |
| 3.   | <b>Battery Fire</b>                  | Burns, shrapnel from exploding battery  | Intelligent UAV battery charger automatically cuts off the power supply  | <input type="checkbox"/> | <input type="checkbox"/>            | <input checked="" type="checkbox"/> |   |
|  |                                      |   | when a short circuit is detected, prevents over charging and will only allow charging when ambient temperature is safe (18°C-28°C). Safe battery management practise (i.e. electrical connections covered at all times, keep batteries dry and within safe temperature range) will also be implemented.  | <input type="checkbox"/> | <input type="checkbox"/>            | <input checked="" type="checkbox"/> |   |
| 4.   | <b>Loss of control of UAV</b>        | Damage to person/property/ vehicle/animal (from e.g. UAV malfunction, pilot error, bad take-off/landing). Most damage is likely to be to UAV. | Small size (35 x 35cm) and weight (<1kg) of UAV minimizes potential damage. Manual control of UAV by pilot, inbuilt return to home function on UAV when comms are lost, automatic warning and return to home when battery is low all minimise risk of crash. Standard operating procedures, operational flight checklists, pilot training (e.g. at least 5 hours flying experience in the field or on simulator, awareness of regulations and familiarity with aircraft) and pre-flight site assessments also minimise risk. Good flight planning by ensuring that UAV is not flown near people, buildings or major roads, will also be enforced to reduce risk. Detailed attention will also be paid to meteorological conditions (in particular wind speed and direction) in order to minimise risk. | <input type="checkbox"/> | <input checked="" type="checkbox"/> | <input type="checkbox"/>            |   |
| 5.   | <b>Loss of transmitter contact</b>   | Damage to person/property/ vehicle/animal   | Ensure transmitter aerial is pointed at UAV at all times (Commander responsibility). If communication between UAV and controller is lost, inbuilt return to home function ensures that UAV returns to home.  | <input type="checkbox"/> | <input type="checkbox"/>            | <input checked="" type="checkbox"/> |   |
| 6.   | <b>Landing in water/trees</b>        | Damage to UAV/tree  | Good flight planning. Increase safety margins around water and wooded areas (avoid completely if possible).  | <input type="checkbox"/> | <input type="checkbox"/>            | <input checked="" type="checkbox"/> |   |
| 7.   | <b>Electrical interference</b>       | Loss of control of UAV  | Investigate site thoroughly for likely signs of interference before flying (e.g. high voltage lines, pylons). Thorough tests of UAV on ground before flight to establish sources of interference (part of operational flight checklist). Do not fly if other UAVs are being operated nearby. Check interference stability on app. If interference is suspected during flight, pilot will land UAV immediately.   | <input type="checkbox"/> | <input type="checkbox"/>            | <input checked="" type="checkbox"/> |   |
| 8.   | <b>Severe weather event</b>          | Loss of UAV   | Thorough check of weather forecast and current weather conditions before flight. If conditions deteriorate during flight, initiate immediate return to home of UAV. Manual control may be required   | <input type="checkbox"/> | <input type="checkbox"/>            | <input checked="" type="checkbox"/> |   |

## 7.5 EXPERIMENT IMAGES



*Figure 16: Images from the IOP on 11th February 2016*

- a) The ground station PC and Tx/Rx for communication with the UAV. The launch/landing side was cordoned off from the public although unleashed pets could not be stopped.*
- b) The UAV mid-flight with the sensor package attached. The additional module is for communication with the ground station Tx/Rx. Prop guards are attached which protect the rotors in the event of a collision.*
- c) Attaching the sensor package (identical to the UAV) to a tethered balloon within RUAO.*
- d) The tethered balloon inside RUAO at a height of 50 m at around 11am. Later in the day the wind speed increased and the balloon began to drift.*

## 7.6 MEASUREMENT VARIABILITY

*Included here as further analysis deemed non-essential to the outcomes of the project.*

In this section the digital SHT sensor the variability of the sensor still contains useful information worth discussing. A method to determine the external influences on the measurements is to look at the variability of the measurements under certain conditions. An increased variability on the UAV data means the UAV is perturbing the measurements, which will allow a hypothesis to be answered. All the data in Table 6 has been averaged to 1 second for fair comparison.

| S.D.         | HEIGHT: (0 m) |            | HEIGHT: (10 m) |            | HEIGHT: (40 m) |            |
|--------------|---------------|------------|----------------|------------|----------------|------------|
|              | RUAO          | BOX AVG    | MAST           | UAV        | BALLOON        | UAV        |
| PRESSURE     | ± 0.06 hPa    | ± 0.04 hPa | ± 0.11hPa      | ± 0.10 hPa | ± 0.19 hPa     | ± 0.12 hPa |
| DIGITAL TEMP | ± 0.03 °C     | ± 0.02 °C  | ± 0.05 °C      | ± 0.07 °C  | ± 0.04 °C      | ± 0.11 °C  |
| THERMISTOR   |               | ± 0.19 °C  | ± 0.18 °C      | ± 0.11 °C  | ± 0.22 °C      | ± 0.07 °C  |
| HUMIDITY     | ± 0.09 %      | ± 0.17 %   | ± 0.53 %       | ± 0.51 %   | ± 0.21 %       | ± 0.34 %   |

*Table 7: Standard deviation over 100 seconds of unchanging measurements for 3 heights. Values for each height are calculated over the same time period. The 0 m data is from the 25/01/16 Stevenson screen test, the 10 m data is from Flight 011, and the 40 m data is from Flight 016. All data is averaged to 1 second to give a fair comparison of variability.*

The thermistor appears to measure more noise than any other sensor which is to be expected since it has the highest measuring frequency and uses analogue ports on the Arduino, which are susceptible to interference. The instruments perform well against RUAO instruments which are taken to be the ground truth.

For 10 m height, pressure variation is less in the UAV which can be attributed to the fact that the maintains altitude with a barometer, so it will actually follow any true pressure perturbation in the atmosphere and dampen the measurement. The digital temperature is more variable on the UAV as expected, since it is oscillating in altitude by ± 0.8 m by the manufacturers definition. The thermistor records higher variability on the mast which may be due to interference from the other sensors on the mast, or the metallic structure itself. Humidity variations are almost equal, which shows the UAV is not affecting atmospheric moisture at this height. Pressure variation variations between the balloon and the UAV at 40 m are even larger, although this can be attributed to the lack of helium in the balloon discussed in section 3.3, which led to the balloon drifting and varying in height between 25



and 50 m. The same variability in temperature is seen at 40 m as it was at 10 m. The thermistor is noisier on the balloon but this can be attributed to the drift issue; the digital sensor has larger variability on the UAV which could mean the balloon is dampening the measurement of temperature. The temperature variability of the UAV at 40 m is larger than that seen at 10 m, which when combined with the increased pressure variability at 40 m, suggests the UAV is fluctuation in height more at 40 m than it was at 10 m. The flow is less turbulent and therefore the aircraft is not oscillating as much, which appears to contradict the previous statement. The humidity variations at 40 m are greater on the UAV, although it is unknown what this may be attributed to. This is only an analysis of one incident, if a statistically sound comparison were to be made, data from more than 30 events would have to be averaged out (Birnbaum and Zuckerman, 1949).